Table 3. *Characteristics of animal models in the subacute phase of coronary artery ligation (day 28)*

	Sham/WT	Sham/R1KO	Sham/R2KO
	Echocardiographic data (under anesthesia)		
n	25	25	25
Heart rate, beats/min	465±16	467±15	471±16
LV EDD, mm	3.4±0.2	3.4±0.2	3.4±0.2
LV ESD, mm	2.3±0.2	2.3±0.2	2.3±0.2
Fractional shortening, %	31.9±2.3	32.3±2.4	32.4±2.7
Infarct wall thickness, mm			
Non-infarct wall thickness, mm	0.80±0.04	0.79±0.04	0.80±0.04
	Hemodynamic data (Millar catheter, under anesthesia)		
n	10	10	10
Heart rate, beats/min	454±24	452±23	457±21
Mean aortic pressure, mmHg	82.5±5.1	81.8±5.0	82.4±4.3
LV EDP, mmHg	2.4±0.5	2.5±0.6	2.5±0.6
$LVdP/dt_{max}$, mmHg/s	7,591±406	7,563±365	7,620±365
$LVdP/dt_{min}$, mmHg/s	5,293±320	5,241±315	5,301±307
	Organ weight data		
n	25	25	25
Body wt, g	26.9±1.6	26.8±1.8	27.1±1.7
Lung wt/body wt, mg/g	5.30±0.37	5.36±0.59	5.41±0.49
Pleural effusion, %	0	0	0
n	15	15	15
LV wt/body wt, mg/g	3.13±0.13	3.19±0.16	3.25±0.19
n	10	10	10
Infarct area, %			
	MI/WT	MI/R1KO	MI/R2KO
	Echocardiographic data (under anesthesia)		
n	35	43	33
Heart rate, beats/min	467±16	469±16	469±18
LV EDD, mm	4.7±0.5*	4.4±0.4*†	5.0±0.5*†
LV ESD, mm	4.1±0.5*	3.7±0.4*†	4.5±0.5*†
Fractional shortening, %	12.3±1.1*	14.9±2.0*†	9.5±1.6*†
Infarct wall thickness, mm	0.39±0.02	0.40±0.03	0.39±0.02
Non-infarct wall thickness, mm	0.89±0.04*	0.90±0.04*	0.89±0.04*
	Hemodynamic data (Millar catheter, under anesthesia)		
n	15	15	14
Heart rate, beats/min	452±31	454±27	455±34
Mean aortic pressure, mmHg	79.3±4.6	78.1±3.9	78.0±5.0
LV EDP, mmHg	8.3±2.4*	6.2±2.1*	12.6±4.8*†
$LVdP/dt_{max}$, mmHg/s	5,051±731*	5,765±802*†	4,362±652*†
$LVdP/dt_{min}$, mmHg/s	3,649±517*	4,171±622*†	3,047±547*†
	Organ weight data		
n	35	43	33
Body wt, g	26.3±1.7	26.1±1.6	27.1±1.9
Lung wt/body wt, mg/g	6.86±2.62*	6.16±1.34	8.10±2.68*†
Pleural effusion, %	17	9	52
n	20	28	19
LV wt/body wt, mg/g	3.78±0.49*	3.66±0.39*	4.26±0.32*†
n	15	15	14
Infarct area, %	53.0±2.8	52.7±2.5	53.1±2.6

Values are means (SD). EDP, end-diastolic pressure; wt, weight. *$P < 0.05$ vs. Sham/WT. †$P < 0.05$ vs. MI/WT.

not differ significantly in MI/R1KO compared with MI/WT mice. Collagen was visualized in LV cross sections with Picrosirius red staining (Fig. 2*C*). Collagen volume fraction, which was increased in MI/WT noninfarct myocardium, was further increased significantly in MI/R2KO mice (Fig. 2*D*).

Increased myocardial expression of TNFR1 by R2KO. Multiprobe RPA was used to evaluate the expression of TNFR1 and TNFR2 in noninfarct myocardium 28 days after MI or sham operation (Fig. 3*A*). The transcript level of TNFR1, which was nullified in R1KO, was not affected by MI but was significantly upregulated in MI/R2KO mice (Fig. 3*B*). In contrast, the transcript level of TNFR2, which was nullified by R2KO, was significantly upregulated by MI and was not further upregulated in MI/R1KO mice.

ELISA was used to evaluate protein levels of TNFR1 and TNFR2 in noninfarct myocardium on *day 28* (Fig. 3*C*). Ablation of the appropriate TNF receptor was evidenced by the fact that TNFR1 and TNFR2 protein levels were not appreciable in

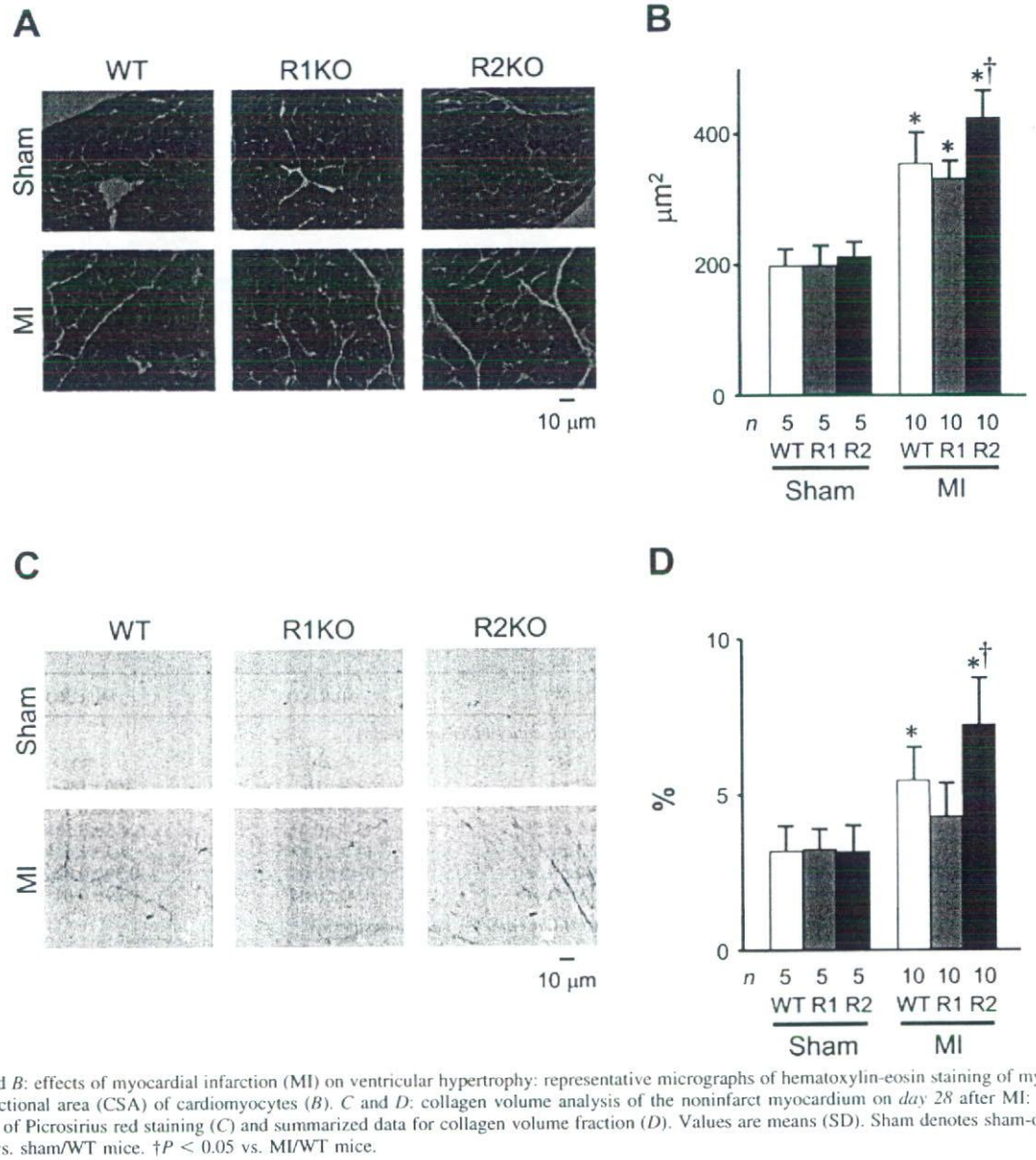

Fig. 2. *A* and *B*: effects of myocardial infarction (MI) on ventricular hypertrophy: representative micrographs of hematoxylin-eosin staining of myocardium (*A*) and cross-sectional area (CSA) of cardiomyocytes (*B*). *C* and *D*: collagen volume analysis of the noninfarct myocardium on *day 28* after MI: representative micrographs of Picrosirius red staining (*C*) and summarized data for collagen volume fraction (*D*). Values are means (SD). Sham denotes sham-operated mice. *$P < 0.05$ vs. sham/WT mice. †$P < 0.05$ vs. MI/WT mice.

the MI/R1KO and MI/R2KO mice, respectively (approximately equal to or lower than the limit of detection, <1.56 pg/mg protein). Consistent with the transcript levels, the cardiac TNFR1 protein level, which was not affected by MI in WT mice, was elevated approximately twofold in MI/R2KO compared with MI/WT mice. In contrast, the cardiac TNFR2 protein level was elevated approximately threefold by MI and was not increased further by R1KO.

To confirm the increased expression of TNFR1 protein in MI/R2KO mice, we performed immunohistochemical staining of TNFR1 (Fig. 4*A*). Consistent with the results of ELISA, TNFR1 staining did not increase in MI/WT mice but increased in MI/R2KO mice. Next, immunohistochemical staining of TNFR2 was performed to confirm the increased expression of TNFR2 protein in MI/WT and MI/R1KO mice (Fig. 4*B*). Consistent with the results of ELISA, TNFR2 staining was increased in response to MI in WT and R1KO mice. The staining was localized to the membrane of cardiomyocytes.

Augmented myocardial expression of proinflammatory cytokines with R2KO. Multiprobe RPA was also used to evaluate the expression of proinflammatory cytokines and chemokines in noninfarct myocardium 28 days after MI or sham operation (Fig. 5*A*). The transcript level of TNF-α was significantly upregulated in noninfarct myocardium in WT and was not modified by the ablation of TNFR1 or TNFR2 (Fig. 5*B*). Transcript levels of IL-6, IL-1β, TGF-β, and MCP-1, which were significantly upregulated in MI/WT noninfarct myocardium, were significantly downregulated in MI/R1KO compared with MI/WT mice. In contrast, transcript levels of IL-6 and IL-1β were significantly further upregulated in MI/R2KO noninfarct myocardium compared with MI/WT mice (Fig. 5*C*).

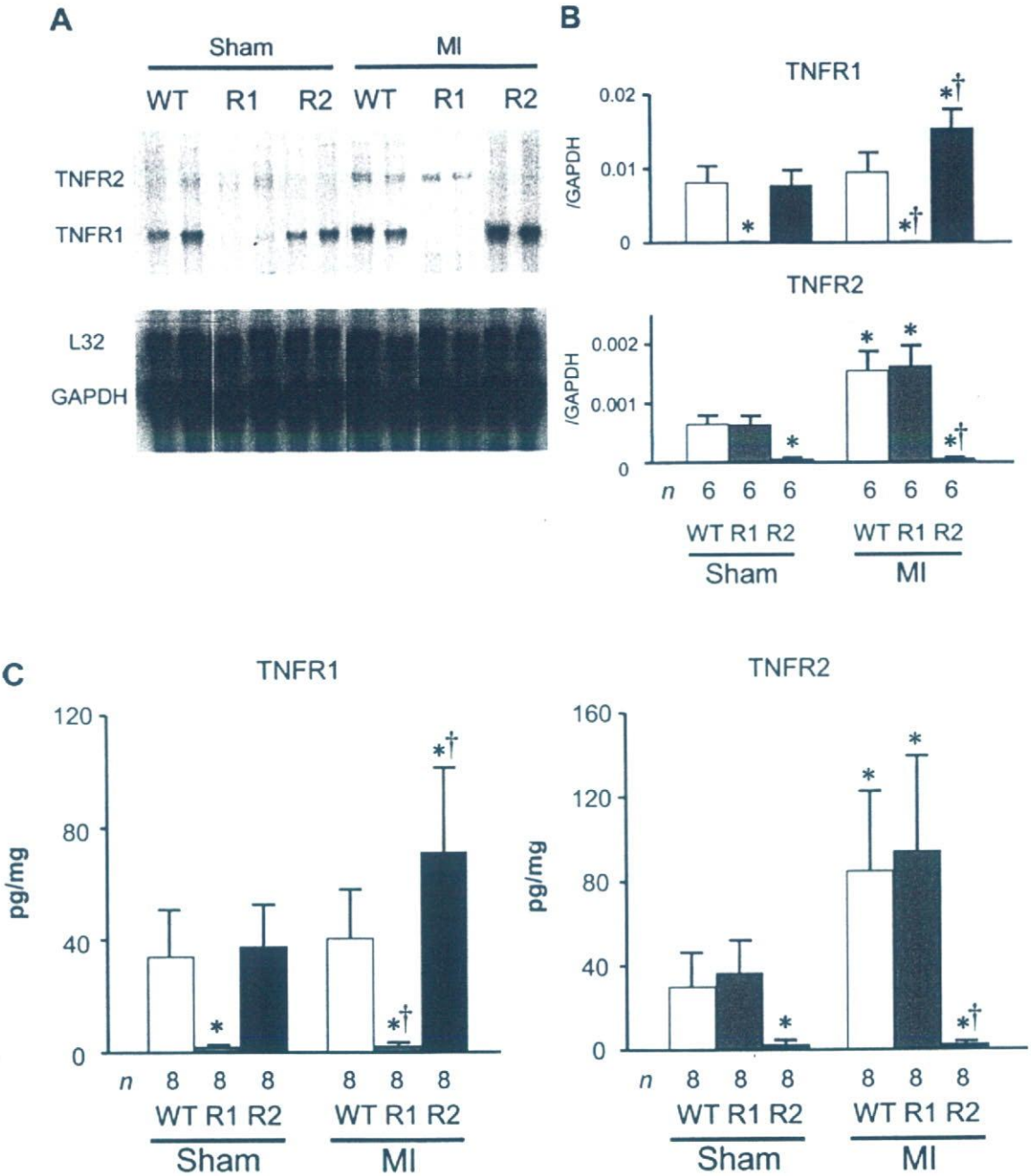

Fig. 3. *A* and *B*: multiprobe RNase protection assays for TNF receptors in noninfarct myocardium on *day 28* after MI: representative gels (*A*) and summarized data for densitometric analysis (*B*). Each value is normalized to that of GAPDH, included in each template set as an internal control. *C*: enzyme-linked immunosorbent assay for TNF receptors. Values are means (SD). *$P < 0.05$ vs. sham/WT mice. †$P < 0.05$ vs. MI/WT mice.

DISCUSSION

Proinflammatory cytokines including TNF-α have been implicated in the pathogenesis of cardiovascular diseases (5, 20). However, the roles of TNF-α in MI remain controversial. Blockade of TNF-α has been reported to be both beneficial (1, 15, 24, 26, 27) and deleterious (2, 18, 22). In the present study, we evaluated the pathophysiological roles of two distinct cell surface receptors (TNFR1 and TNFR2) in the process of infarct healing and cardiac remodeling after MI. Inhibition of TNFR1-mediated pathways attenuated ventricular dysfunction and improved post-MI survival, concomitant with downregulation of other proinflammatory cytokines in noninfarct myocardium. In contrast, inhibition of TNFR2-mediated pathways exacerbated ventricular dysfunction and remodeling, accompanied by upregulation of TNFR1 and other proinflammatory cytokines in noninfarct myocardium. To the best of our knowledge, this study is the first to

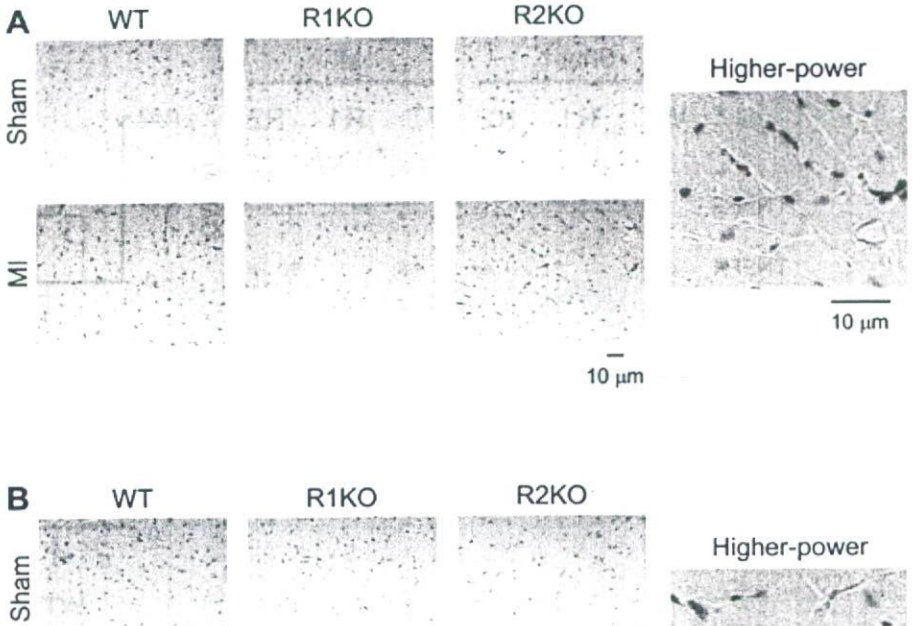

Fig. 4. Immunohistochemistry for TNF receptors in noninfarct myocardium on *day 28* after MI: representative micrographs of TNFR1 staining (*A*) and representative micrographs of TNFR2 staining (*B*). Higher power, ×400 magnification.

document that the ablation of TNFR2 exacerbates ventricular dysfunction and remodeling after MI.

Most biological activities of TNF-α have been considered to be mediated by TNFR1 pathways (33). Three functional domains of TNFR1, the COOH-terminal death domain (28) and the adjacent N-SMase (neutral sphingomyelinase) and A-SMase (acidic sphingomyelinase) activating domains (NSD and ASD, respectively) (25, 34), transfer signals from extracellular TNF-α to intracellular adaptor proteins. The ASD is capable of inducing activation of NF-κB to protect cells against apoptosis (31, 32) and promote inflammation. Ramani et al. (24) have reported that knockout of TNFR1 improves the survival of MI mice. Activation of TNFR1 has been shown to induce various proinflammatory cytokines and chemokines, most of which are considered to be cardiotoxic (5, 20). In the present study, we demonstrated that knockout of TNFR1 suppresses the induction of proinflammatory cytokines and chemokines after MI. These results suggest that TNFR1-mediated pathways are cardiotoxic by inducing various proinflammatory cytokines and chemokines.

Little is known about the roles of TNFR2-mediated pathways. TNFR2 lacks an intracellular death domain (33), suggesting that TNFR2 uses distinct signaling pathways to induce apoptosis (19). Furthermore, whether TNFR2 alone can mediate the activation of NF-κB is controversial (3, 11, 12). Higuchi et al. (10) demonstrated that knockout of TNFR2 increased the mortality by exacerbating the development of heart failure in transgenic mice with cardiac-specific overexpression of TNF-α. In the present study, we have demonstrated that knockout of TNFR2 exacerbates ventricular dysfunction and remodeling after MI together with upregulation of IL-6 and IL-1β. These results suggest that TNF-α may protect the myocardium via TNFR2-mediated pathways. Because knockout of TNFR2 upregulates TNFR1 after MI, the beneficial roles of TNFR2 may be mediated partially by suppression of TNFR1-mediated pathways. The interaction of TNFR1 and TNFR2 pathways may play important roles in MI. In addition, Goukassian et al. (7) recently reported that in a hindlimb ischemia model, endothelial cell apoptosis was increased, and capillary density was decreased in R2KO ischemic tissue. We indeed have evaluated apoptosis in the present study. The number of TdT-mediated dUTP nick end labeling-positive cells increased only slightly in the noninfarct myocardium on *day 28* after MI, regardless of R1KO or R2KO (data not shown). DNA laddering assay also indicated slightly increased apoptosis in noninfarct myocardium and also was not affected by RIKO or R2KO (data not shown). These results indicate that apoptosis in the noninfarct myocardium is not affected by the presence or absence of TNFR1 or TNFR2. The effects of TNFR1 and TNFR2 pathways on nonischemic myocardium after MI may be different from those on ischemic limb tissue.

There are several important aspects to consider in interpreting the results of the present study. First, we used knockout mice to completely block the activation of TNFR1 or TNFR2 pathways. Although growth, appearance, and cardiac function under unstressed conditions seem to be unaffected by R1KO or

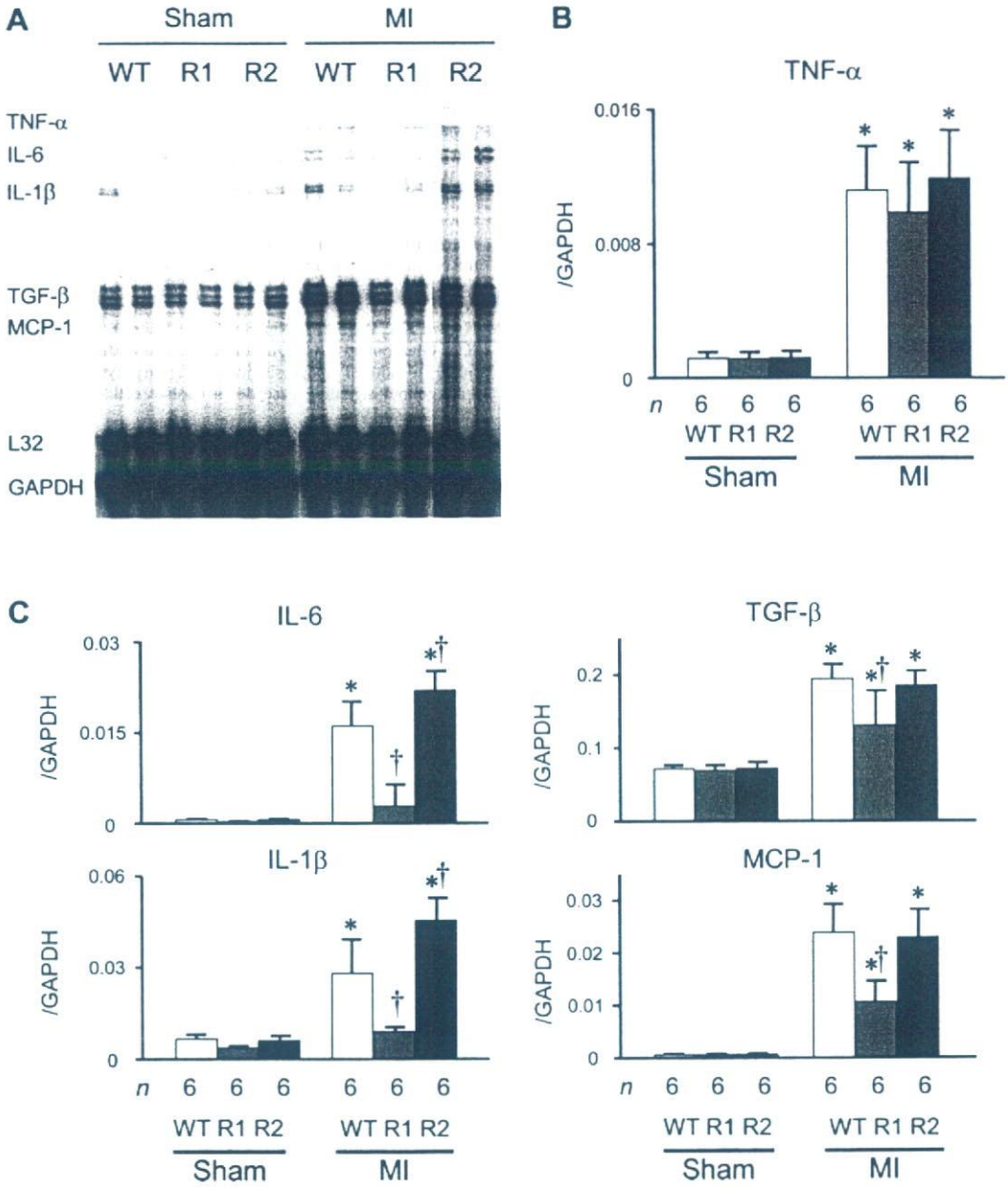

Fig. 5. Multiprobe RNase protection assays for proinflammatory cytokines and chemokines in noninfarct myocardium on *day 28* after MI: representative gels (*A*) and summarized data for densitometric analysis (*B* and *C*). TGF-β, transforming growth factor-β; MCP-1, monocyte chemotactic protein-1. Each value is normalized to that of GAPDH, included in each template set as an internal control. Values are means (SD). $*P < 0.05$ vs. sham/WT mice. $\dagger P < 0.05$ vs. MI/WT mice.

R2KO, the absence of TNFR1 or TNFR2 during embryogenesis and development may alter other signaling pathways to secure physiological growth of these mice. Therefore, caution has to be exercised in interpreting the present results in association with those obtained from clinical trials. Further studies with selective pharmacological ablation of TNFR1 or TNFR2 pathways are required to validate the results of the present study in clinical settings. Second, it is possible that various proinflammatory cytokines play dual roles in post-MI cardiac remodeling and function, as is the case with TNF-α. Therefore, we cannot simply conclude that overexpression of these cytokines in post-MI myocardium is detrimental. Alternatively, overexpression of IL-6 and IL-1β in MI/R2KO mice may represent a compensatory mechanism to salvage the dysfunctional myocardium.

In conclusion, in a murine model of MI, inhibition of TNFR1-mediated pathways attenuates ventricular dysfunction and improves survival with downregulation of other proinflammatory cytokines. In contrast, inhibition of TNFR2-mediated pathways exacerbate ventricular dysfunction and remodeling

with upregulation of TNFR1 and other proinflammatory cytokines in noninfarct myocardium. The findings of the present study may partially explain the unexpected results of anti-TNF-α clinical trials for heart failure. Because TNF-α seems to play both toxic and protective roles in cardiovascular diseases, selective blockade of cardiotoxic TNFR1 may be a candidate therapeutic intervention in clinical practice.

GRANTS

A part of this study was conducted at Kyushu University Station for Collaborative Research. This study was supported by a grant from Kimura Memorial Heart Foundation, a Grant for Research on Cardiovascular Disease from Japan Heart Foundation/Pfizer Pharmaceuticals, Inc., a Grant-in-Aid for Scientific Research from the Japan Society for the Promotion of Science (C15590755), a Health and Labour Sciences Research Grant for Research on Advanced Medical Technology from the Ministry of Health, Labour and Welfare of Japan (H14-Nano-002), a Health and Labour Sciences Research Grant for Research on Medical Devices for Analyzing, Supporting and Substituting the Function of Human Body from the Ministry of Health, Labour and Welfare of Japan (H15-Physi-001), and a Health and Labour Sciences Research Grant for Research on Measures for Intractable Disease from the Ministry of Health, Labour and Welfare of Japan (H17-Nanchi-22).

REFERENCES

1. **Berthonneche C, Sulpice T, Boucher F, Gouraud L, de Leiris J, O'Connor SE, Herbert JM, Janiak P.** New insights into the pathological role of TNF-α in early cardiac dysfunction and subsequent heart failure after infarction in rats. *Am J Physiol Heart Circ Physiol* 287: H340–H350, 2004.
2. **Cai D, Xaymardan M, Holm JM, Zheng J, Kizer JR, Edelberg JM.** Age-associated impairment in TNF-α cardioprotection from myocardial infarction. *Am J Physiol Heart Circ Physiol* 285: H463–H469, 2003.
3. **Chainy GB, Singh S, Raju U, Aggarwal BB.** Differential activation of the nuclear factor-κB by TNF muteins specific for the p60 and p80 TNF receptors. *J Immunol* 157: 2410–2417, 1996.
4. **Chung ES, Packer M, Lo KH, Fasanmade AA, Willerson JT.** Randomized, double-blind, placebo-controlled, pilot trial of infliximab, a chimeric monoclonal antibody to tumor necrosis factor-α, in patients with moderate-to-severe heart failure: results of the anti-TNF Therapy Against Congestive Heart Failure (ATTACH) trial. *Circulation* 107: 3133–3140, 2003.
5. **Feldman AM, Combes A, Wagner D, Kadokami T, Kubota T, Li YY, McTiernan C.** The role of tumor necrosis factor in the pathophysiology of heart failure. *J Am Coll Cardiol* 35: 537–544, 2000.
6. **Finkel MS, Oddis CV, Jacob TD, Watkins SC, Hattler BG, Simmons RL.** Negative inotropic effects of cytokines on the heart mediated by nitric oxide. *Science* 257: 387–389, 1992.
7. **Goukassian DA, Qin G, Dolan C, Murayama T, Silver M, Curry C, Eaton E, Luedemann C, Ma H, Asahara T, Zak V, Mehta S, Burg A, Thorne T, Kishore R, Losordo DW.** Tumor necrosis factor-α receptor p75 is required in ischemia-induced neovascularization. *Circulation* 115: 752–762, 2007.
8. **Hayashidani S, Tsutsui H, Ikeuchi M, Shiomi T, Matsusaka H, Kubota T, Imanaka-Yoshida K, Itoh T, Takeshita A.** Targeted deletion of MMP-2 attenuates early LV rupture and late remodeling after experimental myocardial infarction. *Am J Physiol Heart Circ Physiol* 285: H1229–H1235, 2003.
9. **Hayashidani S, Tsutsui H, Shiomi T, Ikeuchi M, Matsusaka H, Suematsu N, Wen J, Egashira K, Takeshita A.** Anti-monocyte chemoattractant protein-1 gene therapy attenuates left ventricular remodeling and failure after experimental myocardial infarction. *Circulation* 108: 2134–2140, 2003.
10. **Higuchi Y, McTiernan CF, Frye CB, McGowan BS, Chan TO, Feldman AM.** Tumor necrosis factor receptors 1 and 2 differentially regulate survival, cardiac dysfunction, and remodeling in transgenic mice with tumor necrosis factor-α-induced cardiomyopathy. *Circulation* 109: 1892–1897, 2004.
11. **Hohmann HP, Brockhaus M, Baeuerle PA, Remy R, Kolbeck R, van Loon AP.** Expression of the types A and B tumor necrosis factor (TNF) receptors is independently regulated, and both receptors mediate activation of the transcription factor NF-κB. TNFα is not needed for induction of a biological effect via TNF receptors. *J Biol Chem* 265: 22409–22417, 1990.
12. **Hohmann HP, Remy R, Poschl B, van Loon AP.** Tumor necrosis factors-α and -β bind to the same two types of tumor necrosis factor receptors and maximally activate the transcription factor NF-κB at low receptor occupancy and within minutes after receptor binding. *J Biol Chem* 265: 15183–15188, 1990.
13. **Ikeuchi M, Tsutsui H, Shiomi T, Matsusaka H, Matsushima S, Wen J, Kubota T, Takeshita A.** Inhibition of TGF-β signaling exacerbates early cardiac dysfunction but prevents late remodeling after infarction. *Cardiovasc Res* 64: 526–535, 2004.
14. **Irwin MW, Mak S, Mann DL, Qu R, Penninger JM, Yan A, Dawood F, Wen WH, Shou Z, Liu P.** Tissue expression and immunolocalization of tumor necrosis factor-α in postinfarction dysfunctional myocardium. *Circulation* 99: 1492–1498, 1999.
15. **Iversen PO, Nicolaysen G, Sioud M.** DNA enzyme targeting TNF-α mRNA improves hemodynamic performance in rats with postinfarction heart failure. *Am J Physiol Heart Circ Physiol* 281: H2211–H2217, 2001.
16. **Krown KA, Page MT, Nguyen C, Zechner D, Gutierrez V, Comstock KL, Glembotski CC, Quintana PJ, Sabbadini RA.** Tumor necrosis factor α-induced apoptosis in cardiac myocytes. Involvement of the sphingolipid signaling cascade in cardiac cell death. *J Clin Invest* 98: 2854–2865, 1996.
17. **Kubota T, Bounoutas GS, Miyagishima M, Kadokami T, Sanders VJ, Bruton C, Robbins PD, McTiernan CF, Feldman AM.** Soluble tumor necrosis factor receptor abrogates myocardial inflammation but not hypertrophy in cytokine-induced cardiomyopathy. *Circulation* 101: 2518–2525, 2000.
18. **Kurrelmeyer KM, Michael LH, Baumgarten G, Taffet GE, Peschon JJ, Sivasubramanian N, Entman ML, Mann DL.** Endogenous tumor necrosis factor protects the adult cardiac myocyte against ischemic-induced apoptosis in a murine model of acute myocardial infarction. *Proc Natl Acad Sci USA* 97: 5456–5461, 2000.
19. **Lin RH, Hwang YW, Yang BC, Lin CS.** TNF receptor-2-triggered apoptosis is associated with the down-regulation of Bcl-xL on activated T cells and can be prevented by CD28 costimulation. *J Immunol* 158: 598–603, 1997.
20. **Mann DL.** Inflammatory mediators and the failing heart: past, present, and the foreseeable future. *Circ Res* 91: 988–998, 2002.
21. **Mann DL, McMurray JJ, Packer M, Swedberg K, Borer JS, Colucci WS, Djian J, Drexler H, Feldman A, Kober L, Krum H, Liu P, Nieminen M, Tavazzi L, van Veldhuisen DJ, Waldenstrom A, Warren M, Westheim A, Zannad F, Fleming T.** Targeted anticytokine therapy in patients with chronic heart failure: results of the Randomized Etanercept Worldwide Evaluation (RENEWAL). *Circulation* 109: 1594–1602, 2004.
22. **Monden Y, Kubota T, Tsutsumi T, Inoue T, Kawano S, Kawamura N, Ide T, Egashira K, Tsutsui H, Sunagawa K.** Soluble TNF receptors prevent apoptosis in infiltrating cells and promote ventricular rupture and remodeling after myocardial infarction. *Cardiovasc Res* 73: 794–805, 2007.
23. **Pfeffer K, Matsuyama T, Kundig TM, Wakeham A, Kishihara K, Shahinian A, Wiegmann K, Ohashi PS, Kronke M, Mak TW.** Mice deficient for the 55 kd tumor necrosis factor receptor are resistant to endotoxic shock, yet succumb to *L. monocytogenes* infection. *Cell* 73: 457–467, 1993.
24. **Ramani R, Mathier M, Wang P, Gibson G, Togel S, Dawson J, Bauer A, Alber S, Watkins SC, McTiernan CF, Feldman AM.** Inhibition of tumor necrosis factor receptor-1-mediated pathways has beneficial effects in a murine model of postischemic remodeling. *Am J Physiol Heart Circ Physiol* 287: H1369–H1377, 2004.
25. **Schutze S, Potthoff K, Machleidt T, Berkovic D, Wiegmann K, Kronke M.** TNF activates NF-κB by phosphatidylcholine-specific phospholipase C-induced "acidic" sphingomyelin breakdown. *Cell* 71: 765–776, 1992.
26. **Sugano M, Tsuchida K, Hata T, Makino N.** In vivo transfer of soluble TNF-α receptor 1 gene improves cardiac function and reduces infarct size after myocardial infarction in rats. *FASEB J* 18: 911–913, 2004.
27. **Sun M, Dawood F, Wen WH, Chen M, Dixon I, Kirshenbaum LA, Liu PP.** Excessive tumor necrosis factor activation after infarction contributes to susceptibility of myocardial rupture and left ventricular dysfunction. *Circulation* 110: 3221–3228, 2004.
28. **Tartaglia LA, Ayres TM, Wong GH, Goeddel DV.** A novel domain within the 55 kd TNF receptor signals cell death. *Cell* 74: 845–853, 1993.
29. **Tartaglia LA, Weber RF, Figari IS, Reynolds C, Palladino MA Jr, Goeddel DV.** The two different receptors for tumor necrosis factor

mediate distinct cellular responses. *Proc Natl Acad Sci USA* 88: 9292–9296, 1991.

30. **Torre-Amione G, Kapadia S, Lee J, Durand JB, Bies RD, Young JB, Mann DL.** Tumor necrosis factor-α and tumor necrosis factor receptors in the failing human heart. *Circulation* 93: 704–711, 1996.
31. **Van Antwerp DJ, Martin SJ, Kafri T, Green DR, Verma IM.** Suppression of TNF-α-induced apoptosis by NF-κB. *Science* 274: 787–789, 1996.
32. **Wang CY, Mayo MW, Baldwin AS Jr.** TNF- and cancer therapy-induced apoptosis: potentiation by inhibition of NF-κB. *Science* 274: 784–787, 1996.
33. **Wang H, Czura CJ, Tracey KJ.** Tumor necrosis factor. In: *The Cytokine Handbook* (4th ed.), edited by Thomson AW and Lotze MT. San Diego, CA: Acadmic, 2003, p. 837–860.
34. **Wiegmann K, Schutze S, Machleidt T, Witte D, Kronke M.** Functional dichotomy of neutral and acidic sphingomyelinases in tumor necrosis factor signaling. *Cell* 78: 1005–1015, 1994.
35. **Yokoyama T, Vaca L, Rossen RD, Durante W, Hazarika P, Mann DL.** Cellular basis for the negative inotropic effects of tumor necrosis factor-α in the adult mammalian heart. *J Clin Invest* 92: 2303–2312, 1993.

Inducible cAMP Early Repressor Inhibits Growth of Vascular Smooth Muscle Cell

Hideki Ohtsubo, Toshihiro Ichiki, Ryohei Miyazaki, Keita Inanaga, Ikuyo Imayama, Yasuko Hashiguchi, Junichi Sadoshima, Kenji Sunagawa

Objective—The role of inducible cAMP early repressor (ICER), a transcriptional repressor, in the vascular remodeling process has not been determined. We examined whether ICER affects growth of vascular smooth muscle cells (VSMCs).

Methods and Results—Semi-quantitative RT-PCR and Western blot analysis showed that expression of ICER was increased in beraprost (a prostaglandin I_2 analogue)-stimulated VSMCs in a time- and dose-dependent manner. The induction of ICER was inhibited by pretreatment with H89, a protein kinase A (PKA) inhibitor, suggesting that PKA mediates the induction of ICER expression. Beraprost suppressed platelet-derived growth factor–induced thymidine incorporation in VSMCs, which was reversed by transfection of short interfering RNA for ICER, not by scramble RNA. Overexpression of ICER by an adenovirus vector attenuated neointimal formation (intima/media ratio) by 50% compared with overexpression of LacZ. The number of terminal deoxynucleotidyl transferase-mediated dUTP nick end-labeling–positive cells was increased and the number of Ki-67–positive cells was decreased in ICER-transduced artery.

Conclusion—These results suggest that ICER induces apoptosis and inhibits proliferation of VSMCs, and plays a critical role in beraprost-mediated suppression of VSMC proliferation. ICER may be an important endogenous inhibitor of vascular proliferation. (***Arterioscler Thromb Vasc Biol.* 2007;27:1549-1555.**)

Key Words: PGI_2 analogue ■ inducible cAMP early repressor ■ neointimal formation ■ VSMC

Transcription of many cellular genes is regulated by changes of intracellular cAMP levels. The increased cAMP activates protein kinase A (PKA), resulting in the PKA-dependent phosphorylation of nuclear proteins that belong to the cAMP response element (CRE)-binding protein (CREB) family of transcription factors, such as CREB, cAMP response element modulator (CREM), and activating transcription factor-1.[1] Inducible cAMP early repressor (ICER), an isoform of CREM, has a DNA binding domain but lacks a transactivation domain.[2] Therefore, ICER binds to CRE sites but inhibits CRE-dependent gene transcription, which makes ICER serve as a transcriptional repressor. Expression of ICER is inducible in various cell types such as pituitary cells, and cardiac myocytes.[3–6]

Activation of CREB family protein is generally mediated by phosphorylation.[1] Activity of ICER, however, depends on the level of its expression, because ICER dose not contain a PKA-dependent phosphorylation site.[2] Although Yehia et al previously reported that ICER was phosphorylated by mitogen activated protein kinase (MAPK), phosphorylation of ICER affected stability of ICER protein without an effect on ICER activity.[7]

Beraprost, a prostaglandin I_2 (PGI_2) analogue, has antiplatelet and vasodilatory effects.[8,9] Beraprost is, therefore, clinically used for the treatment of arteriosclerosis obliterans and pulmonary hypertension. Beraprost functions through cell surface G protein–coupled PGI_2 receptor designated IP receptor.[10] Activation of IP receptor increases intracellular cAMP level via stimulation of adenylyl cyclase.[11] Activation of adenylyl cyclase increases intracellular cAMP level, which is followed by PKA activation.[11]

It has been reported that beraprost suppresses platelet-derived growth factor (PDGF)-induced DNA synthesis of vascular smooth muscle cells (VSMCs).[12] However, a key regulatory molecule of beraprost-mediated suppression of PDGF-stimulated DNA synthesis has not been determined. The role of ICER in blood vessels and atherogenesis is also poorly characterized. We showed in the present study that beraprost suppresses PDGF-stimulated DNA synthesis through induction of ICER, and overexpression of ICER suppresses neointimal formation in balloon-injured rat carotid artery.

Materials and Methods

Materials

Dulbecco modified Eagle medium (DMEM) was purchased from Gibco BRL, and fetal bovine serum (FBS) were purchased from JRH

Original received October 2, 2006; final version accepted April 16, 2007.

From the Department of Cardiovascular Medicine (H.O., T.I., R.M., K.I., I.I., Y.H., K.S.), Kyushu University Graduate School of Medical Sciences, Fukuoka, Japan; and the Cardiovascular Research Institute (J.S.), University of Medicine and Dentistry of New Jersey.

Correspondence to Toshihiro Ichiki, MD, Department of Cardiovascular Medicine, Kyushu University Graduate School of Medical Sciences, 3-1-1 Maidashi, Higashiku, 812-8582 Fukuoka, Japan. E-mail ichiki@cardiol.med.kyushu-u.ac.jp

Arterioscler Thromb Vasc Biol. **is available at http://www.atvbaha.org** **DOI: 10.1161/ATVBAHA.107.145011**

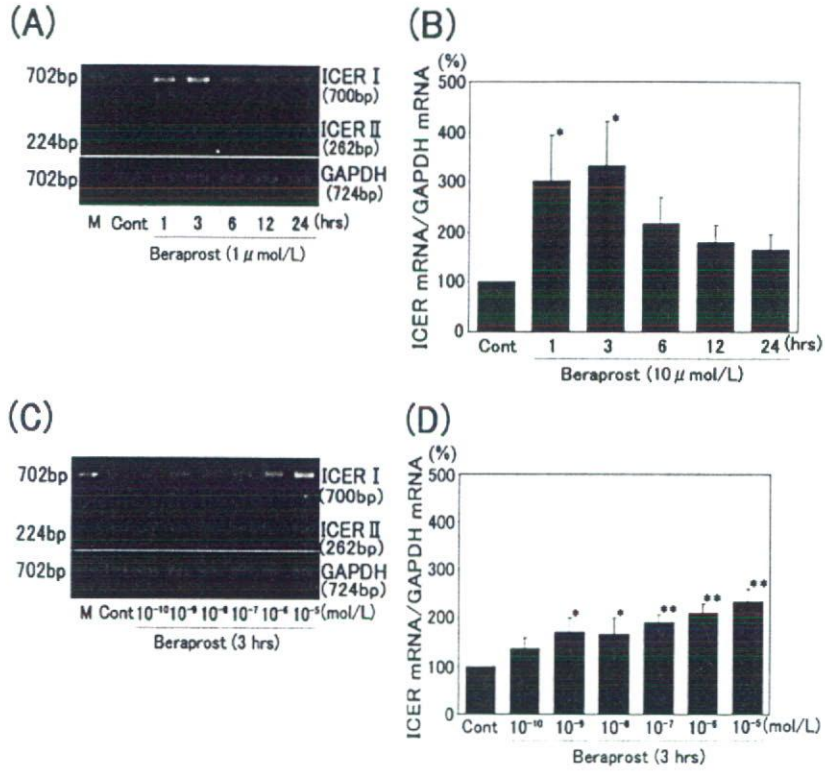

Figure 1. Beraprost induces expression of ICER mRNA. A and B, VSMCs were stimulated with beraprost (1 μmol/L) for various periods as indicated in the figure. C and D, VSMCs were stimulated with beraprost at concentrations varying from 100 pmol/L to 10 μmol/L for 3 hours. Total RNA was isolated, and expression of ICER mRNA and GAPDH mRNA were detected by semiquantitative RT-PCR. A representative photograph of agarose gel analysis is shown. Bar graphs show densitometric analysis of agarose gel stained with ethidiumbromide (n=4). The ratio of ICER to GAPDH is indicated as a percentage of unstimulated control. *P<0.05, **P<0.01 vs control; M, molecular size marker for DNA.

Biosciences Inc. Bovine serum albumin (BSA) was purchased from Sigma Chemical Co. Horseradish peroxidase-conjugated secondary antibodies (anti-rabbit or anti-mouse IgG) were purchased from VECTOR Laboratories Inc. A rabbit polyclonal antibody against CREM-1 for detection of ICER was obtained from Santa Cruz Biotechnology. An anti-CREB antibody was purchased from Cell Signaling Technology. An antibody against Ki-67 antigen was purchased from Dako Cytomation Corporation. Beraprost sodium was provided by Astellas Pharma Inc. Other chemical reagents were purchased from Wako Pure Chemicals unless specifically mentioned.

Cell Culture

VSMCs were isolated from the thoracic aorta of Sprague-Dawley rat by an explant method and maintained in DMEM supplemented with 10% FBS in a humidified atmosphere of 95% air-5% CO_2 at 37°C. VSMCs were cultured until grown to confluence, cultured in DMEM with 0.1% BSA for additional 2 days, and used in the experiment. Cells between passage 5 and 14 were used.

Adenovirus Vector Expressing ICER and LacZ

A recombinant adenovirus vector expressing ICER (AdICER) was reported previously.[13] Confluent VSMCs were washed 2 times with phosphate-buffered saline (PBS) and incubated with AdICER or an adenovirus vector expressing LacZ (AdLacZ) under gentle agitation for 2 hours at room temperature. Then the cells were washed 3 times with PBS, cultured in DMEM with 0.1% BSA for 2 days, and used for the experiments. Multiplicity of infection (moi) indicates the number of virus per cell added to a culture dish.

Semi-Quantitative Reverse Transcription Polymerase Chain Reaction

Total RNA was prepared according to an acid guanidinium-phenol-chloroform extraction method. Total RNA was phenol-chloroform-extracted and ethanol-precipitated. Then, the total RNA (0.4 μg) was reverse-transcribed (RT) using molony murine leukemia virus reverse transcriptase (ReverTra Ace-α kit, TOYOBO) in 4 μL of reaction mixtures. Semi-quantitative PCR was performed with a T3000 Thermocycler (Biometra) according to the manufacturer's instruction. An aliquot of RT-reaction mixture (0.5 μL for amplification of ICER and 0.2 μL for amplification of Glyceraldehyde-3-phosphate dehydrogenase [GAPDH]) was subjected to PCR. The sequences for sense and antisense primers for ICER were 5′-CTT TAT TTT GGA CTG TGG TAC GG-3′and 5′-TAC TAA TCT GTT TTG GGA GAG CA-3′, respectively. GAPDH was used as a reference for the amount of cDNA. The sequences for sense and antisense primers for GAPDH were 5′-TTC TTG TGC AGT GCC AGC CTC GTC-3′ and 5′-TAG GAA CAG GGA AGG CCA TGC CAG-3′, respectively. Appropriate cycles for ICER and GAPDH were determined to confirm the linear amplification of cDNA by PCR (data not shown). Thirty cycles for ICER and 24 cycles for GAPDH were used. The cDNAs of ICER and GAPDH after PCR reaction were electrophoresed on 2% agarose gel, and stained with ethidiumbromide. The density of ICER and GAPDH cDNA visualized by ultraviolet transillumination was quantified with Image Gauge Softwear (Version 3.45).

Western Blot Analysis

VSMCs were lysed in a lysis buffer containing RIPA (100mmol/L sodium, 60mmol/L Na_2HPO_4, 100mmol/L NaF, 10mmol/L EDTA, and 20mmol/L Tris), 1% aprotinin, 0.5% pepstatin A, 1 mmol/L PMSF, and 0.05% leupeptin. Protein concentrations were determined with the bicinchoninic acid protein assay kit (Pierce Chemical Co). Cell lysates were heated in a sample buffer (62.5mmol/L Tris-HCl [pH 6.8], 10% glycerol, 2% SDS, 0.05% bromophenolblue, and 715mmol/L 2-mercaptoethanol) at 95°C for 3 minutes, electrophoresed on 12% SDS-polyacrylamide gel, and transferred to polyvinylidene difluoride membrane (Immobilon-P, Millipore). The blots were blocked with TBS-T (20mmol/L Tris-HCl [pH 7.6], 137mmol/L NaCl, 0.1% Tween 20) containing 5% skim milk at room temperature for 30 minutes. Western blot analysis of ICER and α-tubulin were performed as described previously.[14]

Short Interfering RNA

The annealed form of siRNA of ICER was constructed from a 19 to 21 bp of ICER (NCBI nucleotide accession number S66024) by

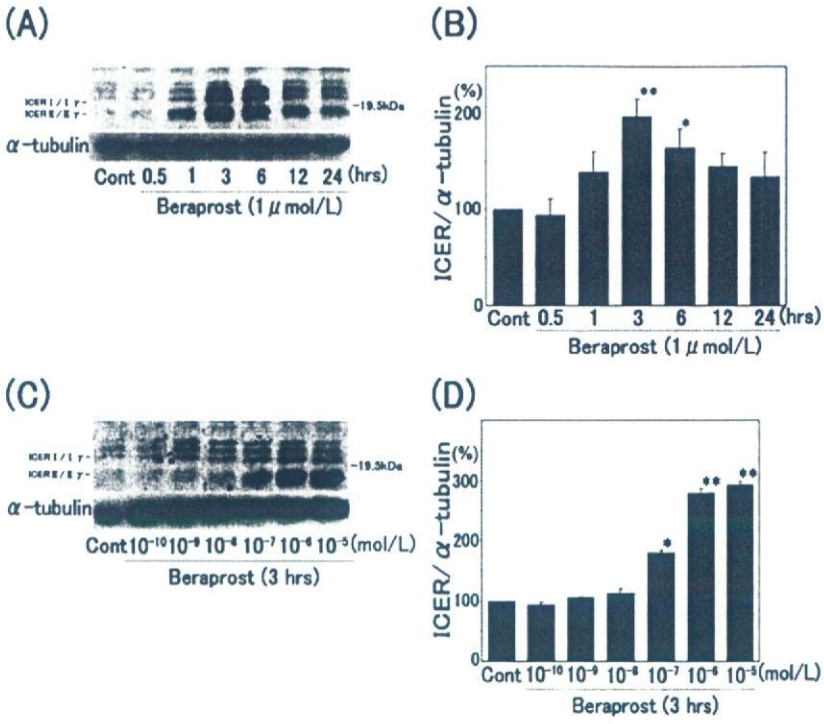

Figure 2. Beraprost induces expression of ICER protein. A and B, VSMCs were stimulated with beraprost (1 μmol/L) for various periods as indicated in the figure. C and D, VSMCs were stimulated with beraprost at concentrations varying from 100 pmol/L to 10 μmol/L for 3 hours. Cell lysate was prepared, and expression of ICER protein was detected by Western blot analysis with an anti-CREM antibody. The membrane was stripped and reprobed with an anti–α-tubulin antibody. A representative blot is shown. Bar graphs show densitometric analysis of Western blots (n=4). The ratio of ICER to α-tubulin is indicated as a percentage of unstimulated control. *P<0.05, **P<0.01 vs control.

Samchully Pharm Co. The optimal ICER sequence was 5′-CUU AUA GAG GAG CUU GAA A-3′. A scrambled sequence, 5′-GAG UAC UUA AGG AUG ACU ATT-3′, that does not contain any significant homology to ICER sequence was used as a control. Introduction of siRNA and scrambled RNA (scRNA) for ICER to VSMCs was performed by lipofection method (Lipofectoamine 2000, Invitrogen Co) according to the manufacturer's instruction.

Measurement of CRE-Dependent Gene Promoter Activity

VSMCs (5×10^5) were prepared in a 6-cm tissue culture dish. Five μg of CRE (3 copies)-luciferase fusion DNA with thymidine kinase gene promoter and 2 μg of β-galactosidase gene were introduced to VSMCs by lipofection method according to the manufacturer's instruction (Invitrogen Co) with siRNA or scRNA for ICER. The cells were cultured in DMEM with 10% FBS for 6 hours, washed twice with PBS, cultured in DMEM with 0.1% BSA for 24 hours, and stimulated with beraprost (10^{-6} mol/L) for 6 hours. Then, the cells were lysed in 200 μL of Reporter lysis buffer (Promega Corporation). Luciferase assay and β-galactosidase assay were performed as described previously[15].

Measurement of DNA Synthesis

siRNA for ICER was introduced into VSMCs by lipofection method. After introduction of siRNA, VSMCs were washed with PBS, and cultured in DMEM with 0.1% BSA for 2 days. VSMCs were pretreated with or without beraprost (1 μmol/L) for 1 hour. VSMCs were, then, stimulated with or without PDGF-BB (50 ng/mL) for 24 hours. The cells were labeled with [^{3}H]-thymidine (PerkinElmer Life Sciences) for the last 4 hours. After labeling, the cells were washed with PBS, fixed in 10% trichloroacetic acid (TCA), and then washed with a mixture of ethanol and ether (2:1). The cells were lysed in 0.5N NaOH, and incorporated [^{3}H]-thymidine was measured by a liquid scintillation counter.

Detection of Apoptosis In Vitro

VSMCs were stimulated with beraprost (1 μmol/L), or infected with AdLacZ (100 moi) or AdICER (100 moi) and maintained in DMEM supplemented with 0.1% BSA for 2 days. VSMCs were isolated through trypsinization. The isolated cells and cells in the medium were collected by centrifugation and stained with propidium iodide (PI). The number of hypodiploid cells was counted from 10 000 cells with Fluorescence-activated cell sorting (FACS; EPICS ALTRA MultiCOMP, Beckman Coulter) analysis as described previously.[16]

Balloon Injury Model and Infection With Adenovirus

All procedures were approved by the institutional animal use and care committee, and were conducted in conformity with institutional guidelines. Balloon injury and infection with adenovirus were performed as described previously.[16] Male Sprague-Dawley rats (Kyndo Co, Japan) (370 to 400g) were anesthetized by intraperitoneal administration of pentobarbital sodium. The left common artery was denuded of the endothelium with 2F Fogarty balloon catheter (Baxter) that was introduced through the external carotid artery. Inflation and retraction of the balloon catheter were repeated 3 times. AdICER (5×10^9 plaque forming unit [PFU]) or AdLacZ (5×10^9PFU) was introduced into the lumen, and the carotid artery was incubated for 15 minutes without blood flow. Then, the viral solution was removed, and the blood flow was restored.

Morphometry and Detection of Apoptosis and Cell Proliferation In Vivo

Morphometry was performed as described previously.[16] Apoptotic cells were detected by the terminal deoxynucleotidyl transferase-mediated dUTP nick end-labeling (TUNEL) method with an apoptosis in situ detection kit (Wako Pure Chemicals). The counterstain was hematoxylin. Cell proliferation was examined by immunohistochemistry with anti–Ki-67 antibody (Dako Inc), which was a nuclear protein preferentially expressed during all active phase of the cell cycle (G_1, S, G_2, and M phases), but absent in resting (G_0) cells.[17] In brief, after the rats were killed, the carotid artery was excised, and fixed with methacarn (methanol: chloroform: acetic acid=6:3:1). After fixation, the carotid artery was embedded into paraffin. The samples were sectioned serially at 4 μm thickness, fixed in acetone, and stained immunohistochemically with an anti–Ki-67 antibody.

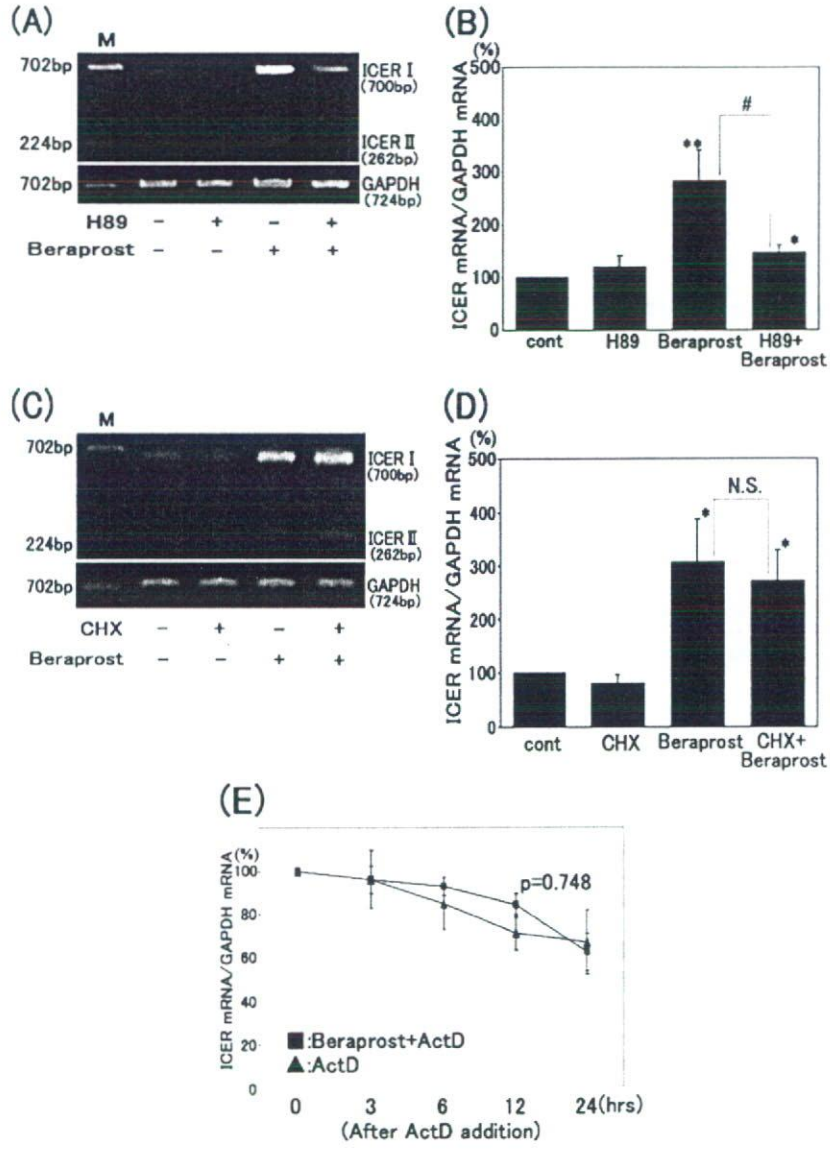

Figure 3. Beraprost induces expression of ICER mRNA through PKA pathway. A and B, VSMCs were stimulated with beraprost (1 μmol/L) for 3 hours after pretreatment with or without H89 (20 μmol/L) for 30 minutes. C and D, VSMCs were stimulated with beraprost (1 μmol/L) for 3 hours after pretreatment with or without cycloheximide (CHX, 10 μg/mL) for 30 minutes. Total RNA was isolated, and expression of ICER mRNA and GAPDH mRNA was determined by semiquantitative RT-PCR. A representative photograph of agarose gel analysis is shown. Bar graph shows densitometric analysis of agarose gel (n=4). The ratio of ICER to GAPDH is indicated as a percentage of unstimulated control. *P<0.05 vs control, **P<0.01 vs control, #P<0.05 vs beraprost. E. VSMCs were stimulated with or without beraprost (1 μmol/L) for 3 hours, then treated with actinomycin D (ActD, 5 μg/mL). Total RNA was prepared at the indicated time points after ActD addition. The expression level of ICER mRNA and GAPDH mRNA was determined by semiquantitative RT-PCR. A line graph shows densitometric analysis of agarose gel (n=4). The ratio of ICER to GAPDH before addition of ActD in each group was set as 100%. Statistical analysis was performed by 2-way ANOVA. A probability value between 2 groups is indicated in the graph.

Quantitative analysis was performed from 100 cells in 5 independent sections from each rat (n=6).

β-Galactosidase Staining In Vivo

The balloon-injured rat carotid artery were stained with the β-galactosidase staining buffer, which contains 5mmol/L $K_4Fe(CN)_6$, 5mmol/L $K_3Fe(CN)_6$, and 1% 5-bromo-4-chloro-3-indole-β-D-galactosidase (X-gal) in PBS, for 6 hours at 37°C. These arteries are fixed in 4% paraformaldehyde and 0.2% gulutaraldehyde in PBS, and embedded into paraffin. The samples were serially sectioned at 4 μm thickness and fixed in acetone. Hematoxylin and eosin were used as counterstaining.

Statistical Analysis

Statistical analysis was performed with 1-way or 2-way ANOVA and Fisher test if appropriate. P<0.05 was considered to be statistically significant. Data are shown as mean±SEM.

Results

Beraprost Induces Expression of ICER mRNA

To examine whether ICER is induced in VSMCs, VSMCs were incubated with beraprost (1 μmol/L) for various periods, and expression of ICER mRNA was determined by semiquantitative RT-PCR method. Two species of ICER mRNA (I and II), which are produced by alternative splicing, were detected. Both bands were taken into account for the densitometric analysis. Maximum expression of ICER mRNA was observed at 3 hours after stimulation (Figure 1A, 1B). Expression of ICER mRNA was dose-dependently increased by beraprost. (Figure 1C, 1D).

Beraprost Induces Expression of ICER Protein

VSMCs were incubated with beraprost (1 μmol/L) for various periods, and expression of ICER protein was determined by Western blot analysis. Maximum expression of ICER protein was observed at 3 hours after stimulation (Figure 2A, 2B). Expression of ICER protein was dose-dependently increased by beraprost (Figure 2C, 2D). Two bands represented ICERI/ICER I γ or ICER II/ICER II γ, which were produced by alternative splicing of γ exon.[18]

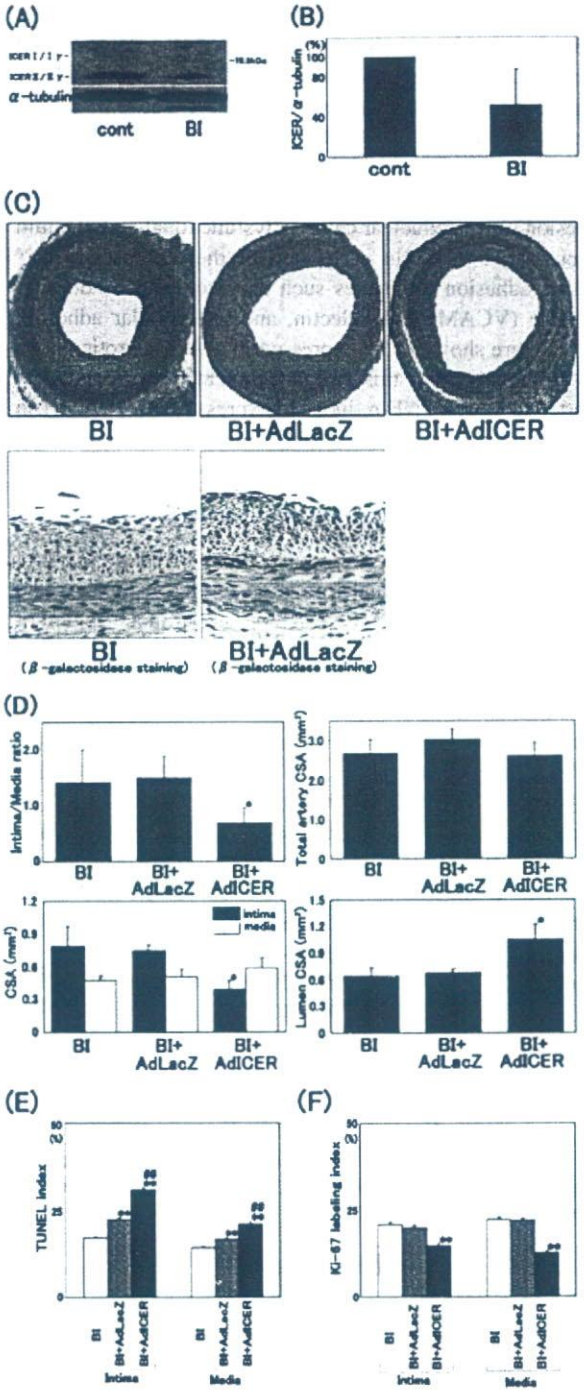

Figure 4. Overexpression of ICER attenuates neointimal formation in balloon-injured artery. A, Western blot analysis of ICER in carotid artery is shown. Control indicates an intact carotid artery. Expression of ICER protein was detected by Western blot analysis. The membrane was stripped and reprobed with an anti-α-tubulin antibody. A representative blot is shown. B, A bar graph shows densitometric analysis of Western blots (n=4). The ratio of ICER to α-tubulin is indicated as a percentage of control. C, Representative micrographs of cross sections of injured carotid arteries stained with hematoxylin-eosin after 14 days of balloon injury are shown in the upper panel. To detect the expression of recombinant adenovirus vector in carotid artery, the β-galactosidase stained-micrographs of control and AdLacZ-infected artery are shown in the lower panel. D, Morphometric analyses after 14 days of balloon injury in these 3 groups are indicated (n=6). *P<0.05 vs balloon injury group (BI) and BI+AdLacZ, CSA: cross-sectional area. E, A bar graph shows the ratio of TUNEL-positive cells to 100 nuclei in the intima or media (n=6). **P<0.01 vs BI, ‡‡P<0.01 vs BI+AdLacZ. F, A bar graph shows the ratio of Ki-67–positive cells to 100 nuclei in the intima or media (n=6). **P<0.01 vs BI.

Beraprost Induces Expression of ICER mRNA Through PKA Pathway

We examined whether PKA pathway mediates induction of ICER mRNA by beraprost. VSMCs were stimulated with beraprost for 3 hours after pretreatment with or without H89, a PKA inhibitor. H89 significantly inhibited the expression of ICER mRNA induced by beraprost (Figure 3A, 3B). To examine whether beraprost-induced expression of ICER mRNA requires de novo protein synthesis, we examined the effect of cycloheximide (CHX). Pretreatment with CHX (10 μg/mL) did not affect induction of ICER mRNA by beraprost (Figure 3C, 3D), suggesting that de novo protein synthesis is not required. We examined whether beraprost affects ICER mRNA stability. Beraprost did not affect the degradation rate of ICER mRNA (Figure 3E), suggesting that beraprost does not affect ICER mRNA stability.

ICER Mediates Beraprost-Induced Suppression of VSMC Proliferation

Previously, it was reported that beraprost inhibited VSMC growth.[12] We examined the role of ICER in beraprost-induced growth suppression. To knockdown of ICER expression, we used siRNA technique. Introduction of siRNA for ICER sufficiently inhibited the expression of beraprost-induced ICER protein, compared with that of scRNA (supplemental Figure IA and IB, available online at http://atvb.ahajournals.org). Neither ICER siRNA nor scRNA affected CREB expression. Introduction of siRNA for ICER significantly upregulated beraprost-induced CRE-luciferase activity (supplemental Figure IC), suggesting that ICER negatively regulates CRE-dependent gene transcription induced by beraprost. Beraprost attenuated [^{3}H]-thymidine incorporation into VSMCs induced by PDGF, and overexpression of ICER also inhibited PDGF-induced VSMCs proliferation. ICER siRNA prevented the inhibitory effect of beraprost (supplemental Figure ID), suggesting that ICER is a key regulatory molecule in the inhibitory effect of beraprost on VSMC proliferation. In addition, overexpression of ICER induced apoptosis of VSMCs. However, beraprost did not increase the number of apoptotic cells (supplemental Figure IE). This may be attributable to that ICER inhibits its expression through negative feedback mechanism,[2] and therefore ICER expression induced by beraprost is transient (Figure 1).

Overexpression of ICER Attenuates Neointimal Formation in Balloon-Injured Artery

A previous report showed that beraprost inhibited neointimal formation after balloon injury.[19] We examined whether overexpression of ICER showed the same effect. We overexpressed ICER in balloon-injured artery by infection with AdICER. Balloon injury decreased endogenous ICER expression (Figure 4A and 4B), although the difference was statis-

tically insignificant. Infection with AdICER suppressed neointimal formation (I/M ratio) and intimal area compared with AdLacZ after 14 days of balloon injury (Figure 4C and 4D). TUNEL index in the neointima of AdICER-infected arteries was significantly increased compared with that of AdLacZ-infected arteries, resulting in an increase in the lumen area (Figure 4E), and Ki-67 labeling index was significantly decreased (Figure 4F) in AdICER-infected arteries.

β-galactosidase staining in control and LacZ transduced artery suggest that infection of adenovirus was successfully performed in injured artery (Figure 4C, lower panels).

Discussion

In the present study, we showed that ICER is inducible in VSMCs by beraprost. We also examined whether ICER is involved in beraprost-induced growth suppression of VSMCs in vitro. The critical role of ICER in beraprost-induced growth suppression was clarified by the experiment using siRNA for ICER, which showed that downregulation of beraprost-induced ICER expression abolished the growth inhibition by beraprost. Overexpression of ICER suppressed neointimal formation in balloon-injured rat carotid artery through induction of apoptosis and inhibition of proliferation.

It was reported that beraprost inhibits neointimal formation by preventing the downregulation of $p27^{Kip1}$ expression, a cyclin-dependent kinase inhibitor that is downregulated by denudation in a canine coronary artery injury model.[19] In this study, beraprost also reduced the number of cells in S phase and increased the number of cells in G1 phase in EGF-stimulated cultured VSMCs, indicating that the cell cycle arrest in G1 phase was induced by beraprost. Lames et al reported that overexpression of ICER induced G2/M arrest in pituitary corticotroph cell line through direct downregulation of the cyclin A, which contains functional CRE sites in the promoter region.[20] In addition, there are several other mechanisms by which cAMP cascades inhibit VSMC growth. Cospedal et al previously reported that cAMP elevating agents inhibited activation of extracellular signal-regulated protein kinases (ERK) 1/2 induced by PDGF.[21] Another group reported that accumulation of cAMP inhibited PDGF-stimulated VSMC growth through apoptosis by induction of p21 and anti-oncogene p53.[22] These results suggest that beraprost may inhibit PDGF-induced proliferation of VSMCs through induction of cell cycle arrest at these 2 cell cycle check points and apoptosis. Because CREB is known to regulate the expression of proliferating cellular nuclear antigen, cyclin A, and cyclin D1, it may be possible that ICER inhibits these cell cycle check points.

We previously reported that CREB mediated tumor necrosis factor (TNF)-α–induced migration of VSMCs.[23] Therefore, it may be possible that overexpression of ICER inhibits VSMC migration from media to neointima, resulting in the attenuation of neointimal formation. Intriguingly, the promoter region of TNF-α that is produced from macrophages as well as VSMCs contains functional CRE site,[24] and another group reported that AII-induced TNF-α expression required CRE-binding site in cardiac fibroblasts,[25] suggesting that TNF-α production from injured artery may be suppressed by ICER overexpression.

Tomita et al reported that overexpression of ICER in cardiac myocytes induced apoptosis through downregulation of Bcl-2, an antiapoptotic molecule.[13] We also reported that overexpression of dominant negative CREB induced VSMCs apoptosis through Bcl-2 downregulation.[15] These data suggest that overexpression of ICER in the injured artery may suppress the Bcl-2 expression in the neointimal VSMCs, and result in an increase in the number of apoptotic cells. Adhesion of mononuclear cells to dysfunctional endothelium is considered to be an early step of the atherosclerosis.[26] Various adhesion molecules such as vascular cell adhesion molecule (VCAM)-1, E-selectin, and intercellular adhesion molecule are shown to be expressed in atherosclerotic lesion and are involved in this cell attachment.[27,28] Beraprost is reported to inhibit TNF-α–induced expression of VCAM-1 in cultured endothelial cells.[2] Because overexpression of dominant negative CREB also inhibits TNF-α–induced VCAM-1 expression,[23] beraprost may inhibit VCAM-1 expression through induction of ICER.

In the present study, we showed that overexpression of ICER inhibited neointimal formation through apoptosis and growth inhibition of VSMCs in vivo. The promoter region of ICER contains 4 CRE-like elements known as cAMP-autoregulatory element.[2] The induction of ICER expression is medicated by CREB, and the induced ICER inhibits ICER induction through CRE site. Thus, this negative feedback system limits the expression of ICER. It is possible that the self-limited induction may weaken the antigrowth effect of endogenous ICER. Although the mechanism is not clear, balloon injury attenuated the expression of ICER, which may contribute to neointimal formation. Therefore the forced expression of ICER in injured artery may be more effective in preventing neointimal formation.

In conclusion, we showed in the present study that ICER suppresses proliferation of VSMCs and induces apoptosis. Our data suggest that ICER may be a novel therapeutic tool for vascular proliferative diseases.

Sources of Funding

This study was supported in part by a Grants-in Aid for Scientific Research from ministry of Education, Culture, Sports, Science, and Technology of Japan (17590742).

Disclosures

None.

References

1. Mayr B, Montminy M. Transcriptional regulation by the phosphorylation-dependent factor CREB. *Nat Rev Mol Cell Biol.* 2001;2:599–609.
2. Molina CA, NS Foulkes, E Lalli, Sassone-Corsi P. Inducibility and negative autoregulation of CREM: an alternative promoter directs the expression of ICER, an early response repressor. *Cell.* 1993;75:875–886.
3. Servillo G, MA Della Fazia, Sassone-Corsi P. Coupling cAMP signaling to transcription in the liver: pivotal role of CREB and CREM. *Exp Cell Res.* 2002;275:143–154.
4. Folco EJ, Koren G. Degradation of the inducible cAMP early repressor (ICER) by the ubiquitin-proteasome pathway. *Biochem J.* 1997;328: 37–43.
5. Wang X, Murphy TJ. The inducible cAMP early repressor ICERIIgamma inhibits CREB and AP-1 transcription but not AT1 receptor gene expression in vascular smooth muscle cells. *Mol Cell Biochem.* 2000; 212:111–119.

6. Don J, Stelzer G. The expanding family of CREB/CREM transcription factors that are involved with spermatogenesis. *Mol Cell Endocrinol.* 2002;187:115–124.
7. Yehia G, Schlotter F, Razavi R, Alessandrini A, Molina CA. Mitogen-activated protein kinase phosphorylates and targets inducible cAMP early repressor to ubiquitin-mediated destruction. *J Biol Chem.* 2001;276: 35272–35279.
8. Umetsu T, T Murata, Tanaka Y, Osada E, Nishio S. Antithrombotic effect of TRK-100, a novel, stable PGI2 analogue. *Jpn J Pharmacol.* 1987;43: 81–90.
9. Hirasawa Y, Nishio M, Maeda K, Yoshida K, Kita Y. Comparison of antiplatelet effects of FK409, a spontaneous nitric oxide releaser, with those of TRK-100, a prostacyclin analogue. *Eur J Pharmacol.* 1995;272: 39–43.
10. Boie Y, Rushmore TH, Darmon-Goodwin A, Grygorczyk R, Slipetz DM, Metters KM, Bramovitz MA. Cloning and expression of a cDNA for the human prostanoid IP receptor. *J Biol Chem.* 1994;269:12173–12178.
11. Lawler OA, Miggin SM, Kinsella BT, Protein kinase A-mediated phosphorylation of serine 357 of the mouse prostacyclin receptor regulates its coupling to G (s) -, to G (i) -, and to G (q) -coupled effector signaling. *J Biol Chem.* 2001;276:33596–33607.
12. Koh E, Morimoto S, Jiang B, Inoue T, Nabata T, Kitano S, Yasuda O, Fukuo K, Gihara TO. Effects of beraprost sodium, a stable analogue of prostacyclin, on hyperplasia, hypertrophy and glycosaminoglycan synthesis of rat aortic smooth muscle cells. *Artery.* 1993;20:242–252.
13. Tomita H, Nazmy M, Kajimoto K, Yehia G, Molina CA, Sadoshima J. Inducible cAMP early repressor (ICER) is a negative-feedback regulator of cardiac hypertrophy and an important mediator of cardiac myocyte apoptosis in response to beta-adrenergic receptor stimulation. *Circ Res.* 2003;93:12–22.
14. Tokunou T, Ichiki T, Takeda K, Funakoshi Y, Iino N, Takeshita A. cAMP response element-binding protein mediates thrombin-induced proliferation of vascular smooth muscle cells. *Arterioscler Thromb Vasc Biol.* 2001;21:1764–1769.
15. Fukuyama K, Ichiki T, Takeda K, Tokunou T, Iino N, Masuda S, Ishibashi M, Egashira K, Shimokawa H, Hirano K, Kanaide H, Takeshita A, Downregulation of vascular angiotensin II type 1 receptor by thyroid hormone. *Hypertension.* 2003;41:598–603.
16. Tokunou T, Shibata R, Kai H, Ichiki T, Morisaki T, Fukuyama K, Ono H, Iino N, Masuda S, Shimokawa H, Egashira K, Imaizumi T, Takeshita A. Apoptosis induced by inhibition of cyclic AMP response element-binding protein in vascular smooth muscle cells. *Circulation.* 2003;108: 1246–1252.
17. Gerdes J, Lemke H, Baisch H, Wacker HH, Schwab U, Stein H. Cell cycle analysis of a cell proliferation-associated human nuclear antigen defined by the monoclonal antibody Ki-67. *J Immunol.* 1984;133: 1710–1715.
18. Bodor J, Spetz AL, Strominger JL, Habener JF. cAMP inducibility of transcriptional repressor ICER in developing and mature human T lymphocytes. *Proc Natl Acad Sci U S A.* 1996;93:3536–3541.
19. Ii M, Hoshiga M, Fukui R, Negoro N, Nakakoji T, Nishiguchi F, Kohbayashi E, Ishihara T, Hanafusa T. Beraprost sodium regulates cell cycle in vascular smooth muscle cells through cAMP signaling by preventing down-regulation of p27 (Kip1). *Cardiovasc Res.* 2001;52: 500–508.
20. Lamas M, Molina C, Foulkes NS, Jansen E, Sassone-Corsi P. Ectopic ICER expression in pituitary corticotroph AtT20 cells: effects on morphology, cell cycle, and hormonal production. *Mol Endocrinol.* 1997;11: 1425–1434.
21. Cospedal R, Lobo M, Zachary I. Differential regulation of extracellular signal-regulated protein kinases (ERKs) 1 and 2 by cAMP and dissociation of ERK inhibition from anti-mitogenic effects in rabbit vascular smooth muscle cells. *Biochem J.* 1999;342:407–414.
22. Hayashi SR, Morishita H, Matsushita H, Nakagami Y, Taniyama T, Nakamura M, Aoki K, Yamamoto J, Higaki J, Ogihara T. Cyclic AMP inhibited proliferation of human aortic vascular smooth muscle cells, accompanied by induction of p53 and p21. *Hypertension.* 2000;35: 237–243.
23. Ono H, Ichiki T, Fukuyama K, Iino N, Masuda S, Egashira K, Takeshita A. cAMP-response element-binding protein mediates tumor necrosis factor-alpha-induced vascular smooth muscle cell migration. *Arterioscler Thromb Vasc Biol.* 2004;24:1634–1639.
24. Roach SK, Lee SB, Schorey JS. Differential activation of the transcription factor cyclic AMP response element binding protein (CREB) in macrophages following infection with pathogenic and nonpathogenic mycobacteria and role for CREB in tumor necrosis factor alpha production. *Infect Immun.* 2005;73:514–522.
25. Sato H, Watanabe A, Tanaka T, Koitabashi N, Arai M, Kurabayashi M, Yokoyama T. Regulation of the human tumor necrosis factor-alpha promoter by angiotensin II and lipopolysaccharide in cardiac fibroblasts: different cis-acting promoter sequences and transcriptional factors. *J Mol Cell Cardiol.* 2003;35:1197–1205.
26. Libby P, Ridker PM, Maseri A. Inflammation and atherosclerosis. *Circulation.* 2002;105:1135–1143.
27. Blankenberg S, Barbaux S, Tiret L. Adhesion molecules and atherosclerosis. *Atherosclerosis.* 2003;170:191–203.
28. Goya K, Otsuki M, Xu X, Kasayama S. Effects of the prostaglandin I2 analogue, beraprost sodium, on vascular cell adhesion molecule-1 expression in human vascular endothelial cells and circulating vascular cell adhesion molecule-1 level in patients with type 2 diabetes mellitus. *Metabolism.* 2003;52:192–198.

Original Article

Inhibition of Balloon Injury–Induced Neointimal Formation by Olmesartan and Pravastatin in Rats with Insulin Resistance

Ming CHEN[1),2)], Toshihiro ICHIKI[1)], Hideki OHTSUBO[1)], Ikuyo IMAYAMA[1)], Keita INANAGA[1)], Ryouhei MIYAZAKI[1)], and Kenji SUNAGAWA[1)]

The combined effect of an angiotensin II type 1 receptor blocker and a 3-hydroxy-3-methylglutaryl-coenzyme A (HMG-CoA) reductase inhibitor on vascular lesion formation in the insulin-resistant state has not been examined. We tested whether or not combined treatment is superior to single-drug treatment for inhibiting vascular lesion formation in insulin-resistant rats. The rats were maintained on a fructose-rich diet for 4 weeks and then treated with olmesartan (1 mg/kg/day) and/or pravastatin (10 mg/kg/day) for 3 weeks. After 1 week of drug treatment, balloon injury of the carotid arteries was performed. Two weeks later, the injured arteries were harvested for morphometry and immunostaining. Olmesartan and pravastatin each modestly attenuated neointimal formation without significant changes in blood pressure or serum lipid levels. The combination of olmesartan and pravastatin significantly suppressed the neointimal formation compared with either monotherapy. The number of terminal deoxynucleotidyl transferase–mediated dUTP nick end-labeling (TUNEL)–positive cells was increased by olmesartan but not by pravastatin. Olmesartan and pravastatin each decreased the number of Ki-67–positive cells, which indicates cell proliferation, to the same extent. The combined treatment increased the number of TUNEL-positive cells but did not affect the number of Ki-67–positive cells. The combined treatment decreased the insulin level and increased the number of circulating endothelial progenitor cells. These results suggest that the combination of olmesartan and pravastatin is beneficial for the treatment of vascular diseases in the insulin-resistant state independently of blood pressure or cholesterol levels. (*Hypertens Res* 2007; 30: 971–978)

***Key Words*: olmesartan, pravastatin, neointimal formation, balloon injury, insulin resistance**

Introduction

Coronary heart disease (CHD) is the leading cause of cardiac mortality and morbidity in the developed countries. Hypertension, hypercholesterolemia, and diabetes mellitus (DM) cause endothelial dysfunction and consequently lead to atherosclerosis. The prevalence of DM is epidemic (*1*). The risk of cardiovascular diseases is two to four times higher in diabetic patients than in the non-diabetic population. Recent studies on the metabolic syndrome (MetS), which is characterized by hypertension, elevated levels of cholesterol and triglyceride, insulin resistance, and central obesity have suggested that these conditions are linked and synergistically

From the [1)]Department of Cardiovascular Medicine, Kyushu University Graduate School of Medical Sciences, Fukuoka, Japan; and [2)]Chongqing University of Medical Sciences, Chongqing, P.R. China.

This study was supported in part by a Kimura Memorial Heart Foundation Research Grant for 2005, a grant from Sankyo Co., and a Grant-in-Aid (No. 17590742) for Scientific Research from the Ministry of Education, Culture, Sports, Science, and Technology of Japan. One of the authors (M.C.) was supported by a Japan-China Sasakawa Medical Fellowship.

Address for Reprints: Toshihiro Ichiki, M.D., Ph.D., Department of Cardiovascular Medicine, Kyushu University Graduate School of Medical Sciences, 3–1–1 Miadashi, Higashi-ku, Fukuoka 812–8582, Japan. E-mail: ichiki@cardiol.med.kyushu-u.ac.jp

Received December 21, 2006; Accepted in revised form May 2, 2007.

enhance the development of DM and atherosclerosis (*2*, *3*). Insulin resistance is believed to play a pivotal role in the development of MetS.

The renin-angiotensin system (RAS) is crucially involved in the development of cardiovascular diseases. Angiotensin (Ang) II is the principal final effector molecule of the RAS. The physiological effects of Ang II are mediated through Ang II receptors (*4*). Several studies have suggested that the beneficial effects of Ang II receptor blocker (ARB) are due to inhibition of the type 1 receptor (AT_1R) function as well as to enhanced stimulation of the type 2 receptor, whose effects are generally believed to be opposite those of AT_1R. Clinical trials have shown that ARB improves the prognosis of patients with acute myocardial infarction (*5*), heart failure (*6*), and renal disease (*7*). And these effects are believed to be independent, at least in part, of their blood pressure (BP)–lowering effects. In addition, most of the recent clinical trials have revealed that ARB treatment decreases the incidence of new-onset diabetes (*8*).

3-Hydroxy-3-methylglutaryl-coenzyme A (HMG-CoA) reductase inhibitors (statins) have been found useful for both primary and secondary prevention of CHD (*9*). In addition to their powerful lipid-lowering effect, it is generally accepted that statins have pleiotropic effects independent of cholesterol-lowering effects, such as enhancement of nitric oxide production, inhibition of smooth muscle proliferation, and anti-inflammatory and antioxidative actions (*10*).

A few reports have suggested that a combination of statins and RAS inhibitors may be more effective than single drug treatment in preventing vascular remodeling after angioplasty. Horiuchi *et al.* reported that fluvastatin enhances the inhibitory effects of valsartan on cuff injury–induced neointimal formation in mice (*11*) and in apolipoprotein E knockout mice (*12*). Recently, Nishikawa *et al.* reported that combination treatment with statin and ARB after coronary stenting is useful for reducing in-stent restenosis (*13*). A recent study showed that ARB and statin improved the anti-atherosclerotic gene expression profiles of internal mammary arteries from patients undergoing coronary artery bypass graft (*14*). However, it has not been examined whether a combination of ARB and statin is effective for inhibiting neointimal formation in an insulin-resistant state. We therefore examined whether or not a combination of ARB and statin is beneficial for preventing balloon injury (BI)–induced neointimal formation in insulin-resistant rats.

Methods

Materials

Olmesartan (Olm), an ARB, and pravastatin (Pra), an HMG-CoA reductase inhibitor, were gifts from Sankyo Co. (Tokyo, Japan). A 2F Fogarty balloon catheter was purchased from Baxter (Deerfield, USA). Olm was dissolved in methylcellulose and diluted in distilled water (final concentration 1 mg/mL). Pra was dissolved in distilled water (final concentration 10 mg/mL).

Animal Model

All procedures and animal care were approved by the Committee on Ethics of Animal Experiments, Kyushu University, and were conducted according to the animal care guidelines of the American Physiological Society. Male Sprague-Dawley (SD) rats at 7 weeks old were divided into two groups. One group was fed a standard rat chow containing 60% vegetable starch, 5% fat, and 24% protein (control group). The other group was fed a fructose-rich chow containing 60% fructose, 5% fat, and 20% protein for 4 weeks, which induced an insulin-resistant state (fructose group) (*15*). The fructose group rats were further divided into a sham operation (Sham) group, a BI group, a BI+Olm group, a BI+Pra group, and a BI+Olm+Pra group. The drugs were given orally by gastric gavage once a day, which was started 1 week before BI and continued for 2 weeks after BI. The rats were fed a fructose-rich diet during drug treatment. Olm was given at a dose of 1 mg/kg/day, which is reported not to affect BP level (*16*). Pra was given at a dose of 10 mg/kg/day, which does not affect serum lipid level (*17*). On the last day of the experiments, rats were kept fasting for 12 h and then sacrificed.

Serum concentrations of glucose, triglyceride (TG), total and low-density lipoprotein cholesterol (TC and LDL-C, respectively), and insulin were measured. Systolic BP (SBP) and heart rate (HR) were measured using the tail-cuff method (UR-5000; Ueda Industries, Tokyo, Japan).

BI of Rat Carotid Artery

The rats were anesthetized by intraperitoneal injection of pentobarbital sodium at the age of 12 weeks. The left common carotid artery was denuded of the endothelium with a 2F Fogarty balloon catheter introduced through the external carotid artery (*18*). Inflation and retraction of the balloon catheter were conducted three times. Then the balloon was removed and the external carotid artery was ligated. Sham operation was performed without BI.

Morphometry and Immunostaining

Two weeks after BI, rats were euthanized with a lethal dose of pentobarbital, and the carotid arteries were fixed by perfusion at 100 mmHg with 4% formaldehyde *via* an 18G intravenous cannula placed retrogradely in the abdominal aorta. The arteries were additionally fixed by immersion in the same fixative used for perfusion. The arteries were excised and then embedded in paraffin. Sections were stained with hematoxylin and eosin. The balloon-injured carotid arteries with intact internal elastic lamina were subjected to morphometry for assessing the intima/media (I/M) ratio. Immunohistochemistry was performed using a denoted primary antibody and a commercially

Table 1. BW, BP and HR before and after Fructose Rich Diet

Group	Weeks	*n*	BW (g)	SBP (mmHg)	HR (/min)
Control	7	16	222±15	111±8	352±21
Control	11	8	353±10†	110±7	345±16
Fructose	11	8	413±22†‡	112±8	342±16

Data are expressed as mean±SD. †$p<0.05$ *vs.* control at 7-weeks. ‡$p<0.05$ *vs.* control at 11-weeks. BW, body weight; SBP, systolic blood pressure; HR, heart rate.

Table 2. Biochemical Analysis of Serum in Control and DM Rats

Group	Weeks	*n*	Glucose (mg/dL)	TC (mg/dL)	LDL-C (mg/dL)	TG (mg/dL)	Insulin (ng/mL)
Control	7	8	128±7	54±6	5±0.5	22±7	0.7±0.2
Control	11	8	134±12	60±10	9±4	37±18	1.0±0.3
Fructose	11	8	177±23‡	398±32‡	87±30‡	75±26‡	4.4±0.7‡

Data are expressed as mean±SD. ‡$p<0.05$ *vs.* control at 11-weeks. TC, total cholesterol; LDL-C, low density lipoprotein cholesterol; TG, triglyceride.

Table 3. BW, BP and HR at 14 Weeks

Group	*n*	BW (g)	SBP (mmHg)	HR (/min)
Control+Sham	8	405±20	113±9	340±18
Control+BI	8	410±23	112±7	336±20
Fructose+Sham	8	416±18	114±9	336±19
Fructose+BI	8	428±18	113±7	344±35
Fructose+BI+Olm	8	405±20	110±6	337±14
Fructose+BI+Pra	8	422±16	114±8	333±13
Fructose+BI+Olm+Pra	8	406±25	108±8	335±19

Data are expressed as mean±SEM. BW, body weight; SBP, systolic blood pressure; HR, heart rate; BI, balloon injury; Olm, olmesartan; Pra, pravastatin.

Table 4. Biochemical Analysis of Serum at 14 Weeks

Group	*n*	Glucose (mg/dL)	TC (mg/dL)	LDL-C (mg/dL)	TG (mg/dL)	Insulin (ng/mL)
Control+Sham	8	133±13	63±12	8±5	39±12	1.0±0.4
Control+BI	8	138±5	61±10	9±5	42±13	1.1±0.4
Fructose+Sham	8	186±25‡	401±42‡	79±21‡	77±18‡	3.8±.6‡
Fructose+BI	8	174±46‡	382±63‡	75±23‡	83±14‡	3.9±.8‡
Fructose+BI+Olm	8	198±30‡	409±74‡	83±31‡	77±14‡	3.4±.9‡
Fructose+BI+Pra	8	222±34‡	357±55‡	69±25‡	70±27‡	3.2±.8‡
Fructose+BI+Olm+Pra	8	176±25‡	324±42‡	56±18‡	59±18‡	1.1±0.4″

Data are expressed as mean±SEM. ‡$p<0.05$ *vs.* control (Sham or BI), ″$p<0.01$ *vs.* other fructose groups. TC, total cholesterol; LDL-C, low density lipoprotein cholesterol; TG, triglyceride; BI, balloon injury; Olm, olmesartan; Pra, pravastatin.

available detection system (Dako Glostrup, Denmark). The extent of neointimal formation was quantified by computed planimetry of histologically stained sections. The cross-sectional areas of the blood vessel layers including the lumen area, intima area, and medial area were quantified at three different sections (proximal, middle, and distal). The ratio of Ki-67–positive cells to total nucleated cells was expressed as the Ki-67 index.

Detection of Apoptosis

Apoptotic cells were detected by the terminal deoxynucleotidyl transferase–mediated dUTP nick end-labeling (TUNEL) method with an Apoptosis *in situ* Detection Kit (Wako Pure

Chemical Industries, Osaka, Japan). The counterstain was done with hematoxylin. Quantitative analysis was performed in five independent sections in each rat ($n=5$). The ratio of TUNEL-positive cells to total nucleated cells was expressed as the TUNEL index.

Isolation of Peripheral Blood Mononuclear Cells and Identification of Endothelial Progenitor Cells

Rat mononuclear cells (MNCs) were initially isolated from peripheral buffy coat blood in a Histopaque-1083 (Sigma-Aldrich, St. Louis, USA). MNCs were then suspended in EGM-2 (Cambrex Bio Science, East Rutherford, USA), placed on a plate coated with collagen type I (Becton Dickinson, Franklin Lakes, USA) and incubated for 4 days. To detect the uptake of 1,1′-dioctadecyl-3,3,3′,3′-tetramethylindocarbocyanine–labeled acetylated low-density lipoprotein (DiLDL; Biomedical Technologies, Stoughton, USA), cells were incubated with DiLDL (10 μg/mL) at 37°C for 4 h. Cells were then fixed with 0.5% paraformaldehyde for 10 min, and lectin staining was performed by incubation with fluorescein isothiocyanate (FITC)–labeled Bandeiraea simplicifolia agglutinin BS-I (lectin, 20 μg/mL; Sigma-Aldrich) at 4°C overnight. After the staining, samples were viewed with an inverted fluorescent microscope (IX71; Olympus, Tokyo, Japan). Dual-stained cells positive for both lectin and DiLDL were judged to be endothelial progenitor cells (EPCs) (*19*) and the number of dual-stained cells was counted per dish with a blinded investigator by 15 randomly selected high-power fields (×200).

Statistical Analysis

Statistical analysis was performed with one-way ANOVA and Fisher's test if appropriate. $p<0.05$ was considered to be statistically significant. Data are shown as means±SEM.

Results

Effect of Fructose-Rich Diet

BP and HR were measured before and after the rats were maintained on normal or fructose-rich chow for 4 weeks (Table 1). The body weight (BW) of the fructose group was significantly higher than that of the control group. However, BP and HR were not significantly different between the control and fructose groups. Biochemical analysis of serum showed that levels of TC, LDL-C, and TG were higher in the fructose group than in the control group (Table 2). It was supposed that the majority of the increased cholesterol was high-density lipoprotein (HDL). The increase in insulin level with an increase in blood glucose level suggests that these rats are insulin-resistant.

At the end of the experiments (14 weeks of age), BW, BP, and HR did not differ significantly among the groups (Table 3). The biochemical analysis at 14 weeks of age revealed that drug treatment did not significantly affect serum levels of glucose or lipids (Table 4). The combination of Olm and Pra, however, significantly decreased serum insulin levels compared with the other fructose-fed groups, suggesting that insulin sensitivity was improved.

BI of Rat Carotid Artery

The hematoxylin-eosin (HE) staining showed that the extent of neointimal formation after BI in fructose-fed rats was the same as that of control rats (Fig. 1). Olm or Pra modestly inhibited neointimal formation. The combination of Olm and Pra was more effective than single drug treatment at inhibiting neointimal formation.

Apoptosis and Proliferation

The TUNEL positively stained cells, which indicate apoptotic cells, was increased in the neointima (Fig. 2A, white bars) of the Olm-treated group. Pra did not affect the number of TUNEL-positive cells. However, the addition of Pra to Olm significantly increased the number of TUNEL-positive cells (Fig. 2A). The same tendency was observed in the media (filled bars), although the absolute number of TUNEL-positive cells in the media was small.

The number of Ki-67–positive cells, which indicates cell proliferation, was increased in the neointima of fructose-fed rats. The number of Ki-67–positive cells was decreased in Olm to the same extent as in Pra (Fig. 2B). However, a synergistic decrease in Ki-67–positive cells was not observed in the combination treatment group. Very few Ki-67–positive cells were observed in the media, and there was no significant difference in the number of Ki-67–positive cells among the groups (data not shown). These data may suggest that the reduction in the neointimal area by the combination treatment is due to an increase in the number of apoptotic cells.

Effect on the Number of EPCs

EPCs are believed to participate in the recovery of endothelium of injured artery. We therefore measured the number of EPCs in the MNCs from these control and fructose-fed rats at the end of the experiments (Fig. 3A). The number of EPCs in the fructose-fed rats was significantly decreased (Fig. 3B). BI significantly increased the number of EPCs in both the control and fructose groups. Neither Olm nor Pra alone had any effect on the number of EPCs in the fructose group. However, the combination treatment significantly increased the number of EPCs.

Discussion

Although we hypothesized that the extent of neointimal formation after BI would be exaggerated in the insulin-resistant

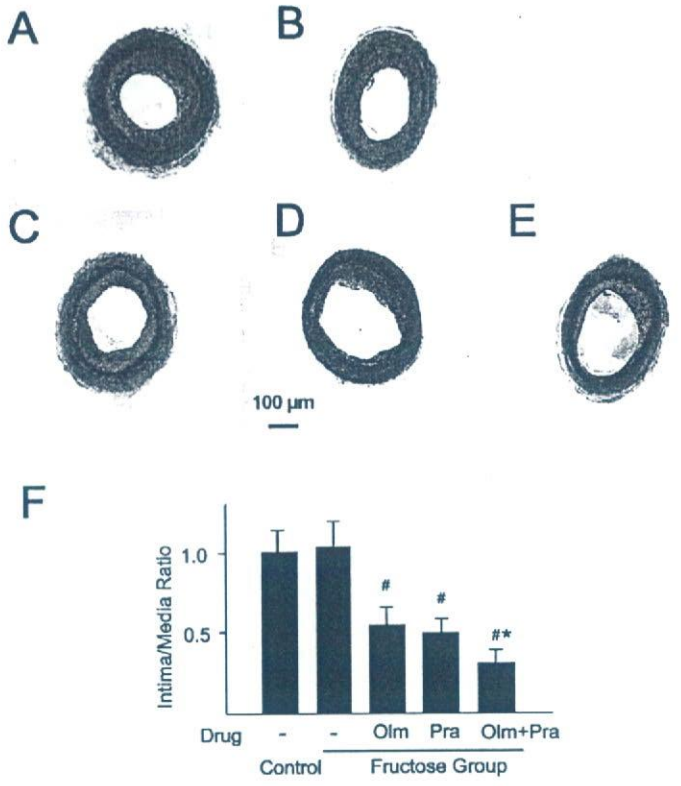

Fig. 1. *Neointimal formation in the carotid artery of control and fructose-fed rats. Representative microphotographs of hematoxylin-eosin staining of carotid artery after 14 days of balloon injury are shown. A: control; B: fructose group; C: fructose+Olm group; D: fructose+Pra group; E: fructose+Olm+Pra group, F: Bar-graph indicates I/M ratio. The values are expressed as means ±SEM. n = 8. #p < 0.05 vs. control. *p < 0.05 vs. Olm or Pra group and p < 0.01 vs. control.*

state, this was not the case. The present data and previous results (*11*) suggest that insulin resistance induced by fructose feeding has little effect on BI-induced neointimal formation, which ARB and statin synergistically suppressed to the same extent in the control and fructose-fed rats.

It has been reported that feeding rats a fructose-rich diet induces insulin resistance and hypertension (*15*). Our data showed that both blood glucose and insulin levels were elevated in rats after they were fed a fructose-rich diet for 4 weeks, suggesting that an insulin-resistant state was established. However, the BP level was not changed. A recent paper showed that a fructose-rich diet did not affect BP level (*20*), which is consistent with our results. The mechanism explaining this difference is not yet clear. It is also difficult to explain the increased lipid levels in the fructose-fed rats. The ingredients of the fructose-rich diet used in our experiment are almost the same as those used in the previous studies (*20, 21*), which reported no significant increase in total cholesterol level but an increase in triglyceride level. Although the mechanism for the increase in cholesterol levels is not clear, Pra did not show a significant effect on cholesterol level in the fructose-fed rats, indicating that a comparison among the fructose groups is possible.

Olm at doses that decrease BP was reported to improve insulin resistance in fructose-fed rats (*21*). Our data, however, indicated that Olm at a dose without BP change did not affect insulin or glucose levels. Intriguingly, the combination of Olm and Pra significantly decreased insulin levels, although Pra alone did not affect insulin levels. The mechanism underlying this combination effect is not clear. One of the possible common target molecules of ARB and statin is Rho-kinase. Ang II is reported to activate the Rho–Rho kinase pathway (*22, 23*). Thus, ARB prevents Ang II–induced Rho-kinase activation. And a recent report suggested that Rho-kinase phosphorylates the serine residue of IRS-1, which inhibits insulin signaling and results in insulin resistance (*23*). Statins are known to inhibit activation of Rho by inhibiting geranylgeranylation (*24*). Actually, it was reported that fluvastatin, another HMG-CoA reductase inhibitor, prevented Ang II–induced cardiac hypertrophy through the inhibition of Rho-kinase (*25*). Therefore, it may be possible that a combination of Olm and Pra synergistically suppresses the Rho–

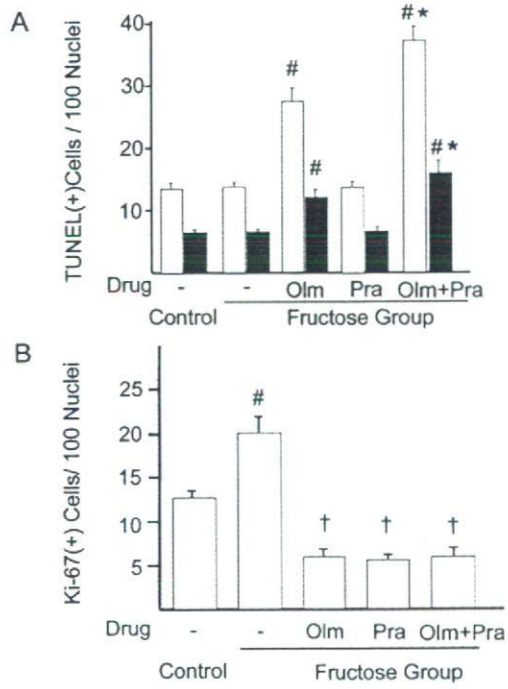

Fig. 2. *Apoptosis and proliferation of VSMC in the injured artery. TUNEL staining and immunohistochemical analysis for Ki-67 staining were performed in cross sections of carotid artery 14 days after balloon injury. A: TUNEL index of the intima (white bars) or media (black bars) is indicated (n = 5). B: Ki-67–positive index of intima (white bars) is indicated. Because there were so few Ki-67–positive cells in the media, these are not indicated in the graph. The values are expressed means ±SEM. #p < 0.05 vs. control. *p < 0.05 vs. Olm. †p < 0.05 vs. control and p < 0.01 vs. fructose group without drug. n = 5.*

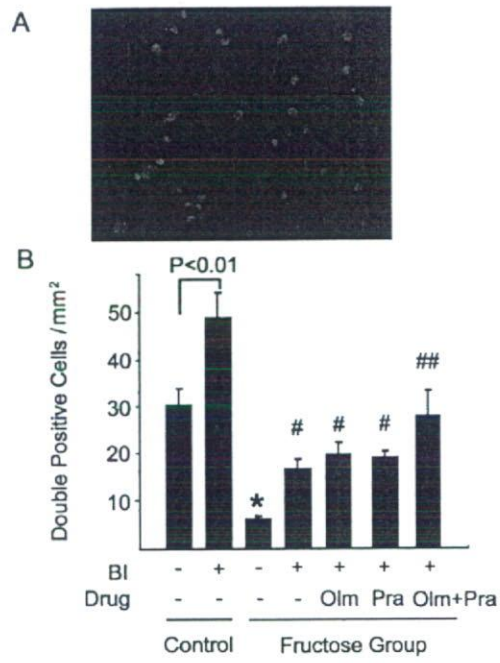

Fig. 3. *The number of endothelial progenitor cells. A: A representative microphotograph of attached mononuclear cells stained with FITC-lectin (green) and incorporating DiI-LDL (red). Part of the microscopic field is enlarged. B: The number of double-positive cells is counted as EPCs. The bar graph indicates the number of EPCs in each group. The values are expressed as means ±SEM. p < 0.05 vs. fructose without BI. *p < 0.05 vs. control without BI. #p < 0.05 vs. fructose group without BI. ##p < 0.01 vs. fructose group without BI and p < 0.05 vs. other fructose with BI groups. n = 5–8.*

Rho kinase pathway and improves insulin resistance.

Contradictory results were reported about the effects of Pra, a hydrophilic statin that penetrates the cell membrane poorly, on vascular smooth muscle cells (VSMC) proliferation and apoptosis. Pra was found to have a minimal effect on the inhibition of VSMC proliferation and the induction of apoptosis, whereas substantial effects were observed with fluvastatin or simvastatin (*26*). However, a recent report showed that Pra at a relatively high dose induces apoptosis and growth inhibition of VSMC, possibly through $p27^{Kip1}$ and phosphatidylinositol-3 kinase (PI-3K) (*27*). Because Ang II is known to activate PI-3K, the combination of Pra and Olm may synergistically inhibit this pathway. However, the mechanisms of the differential effect of the combined therapy on the TUNEL index and Ki-67 index is not yet clear. Further investigation is needed.

The combination of Olm and Pra was also more effective in recruiting EPCs. It was reported that statin-induced EPC mobilization requires increased endothelial nitric oxide (NO) bioavailability (*28*). Because Ang II induces production of reactive oxygen species, which quench NO, the combination of ARB and statin may increase the NO bioavailability, resulting in increased EPC recruitment. Indeed, a recent study showed that a combination treatment of Olm and Pra synergistically improved endothelium-dependent vasodilation and reduced the level of thiobarbituric acid–reactive substances in salt-loaded Dahl salt-sensitive hypertensive rats compared with treatment with either drug alone, suggesting NO has a role in the combined treatment (*29*).

However, the contribution of EPCs to the reduction of neointimal formation is not clear from this study because we did not examine whether or not these cells were incorporated into the regenerated endothelium of the injured vessel. In addition, the number of EPCs in the control BI group, which has the largest neointimal area, is the highest among all groups. Interestingly, it was reported that recruitment of vascular progenitor cells to vascular lesions is injury-dependent (*30*). Tanaka *et al.* (*30*) showed that bone marrow cells were